Supplementary Information

Preparation of PVDMA/PEI Polymeric Films Functionalized with Amino Acids and Their Study on Adhesion and Proliferation of *Escherichia coli*

Alberto Pérez-Zamora,[a] Ignacio A. Rivero,*[,a] Martha E. Ávila-Cossío,[a] Patricia L. A. Muñoz-Muñoz,[b] Rosa E. Mares-Alejandre,[b] Marco A Ramos-Ibarra[b] and Karla A. Espinoza[a]

[a]Centro de Graduados e Investigación en Química, Instituto Tecnológico de Tijuana, Tecnológico Nacional de México, 22510 Tijuana, Baja California, México

[b]Facultad de Ciencias Químicas e Ingeniería, Universidad Autónoma de Baja California, Calzada Universidad 14418, 22390 Tijuana, Baja California, México

*e-mail: irivero@tectijuana.mx

Alberto Pérez-Zamora: 0009-0000-6408-6059
Ignacio A. Rivero: 0000-0003-4920-6379
Martha E. Avila Cossio: 0009-0002-6229-6428
Patricia L. A. Muñoz-Muñoz: 0000-0001-8303-6305
Rosa E. Mares-Alejandre: 0000-0001-6102-6966
Marco A. Ramos-Ibarra: 0000-0002-8950-2079
Karla A. Espinoza: 0000-0001-9969-2681

Spectroscopy of compounds

2-Acrylamido-2-methylpropanoic acid

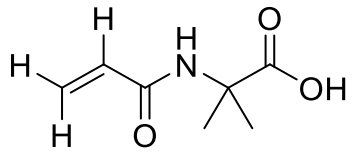

(**1**)

Figure S1. Structure of 2-acrylamido-2-methylpropanoic acid (**1**).

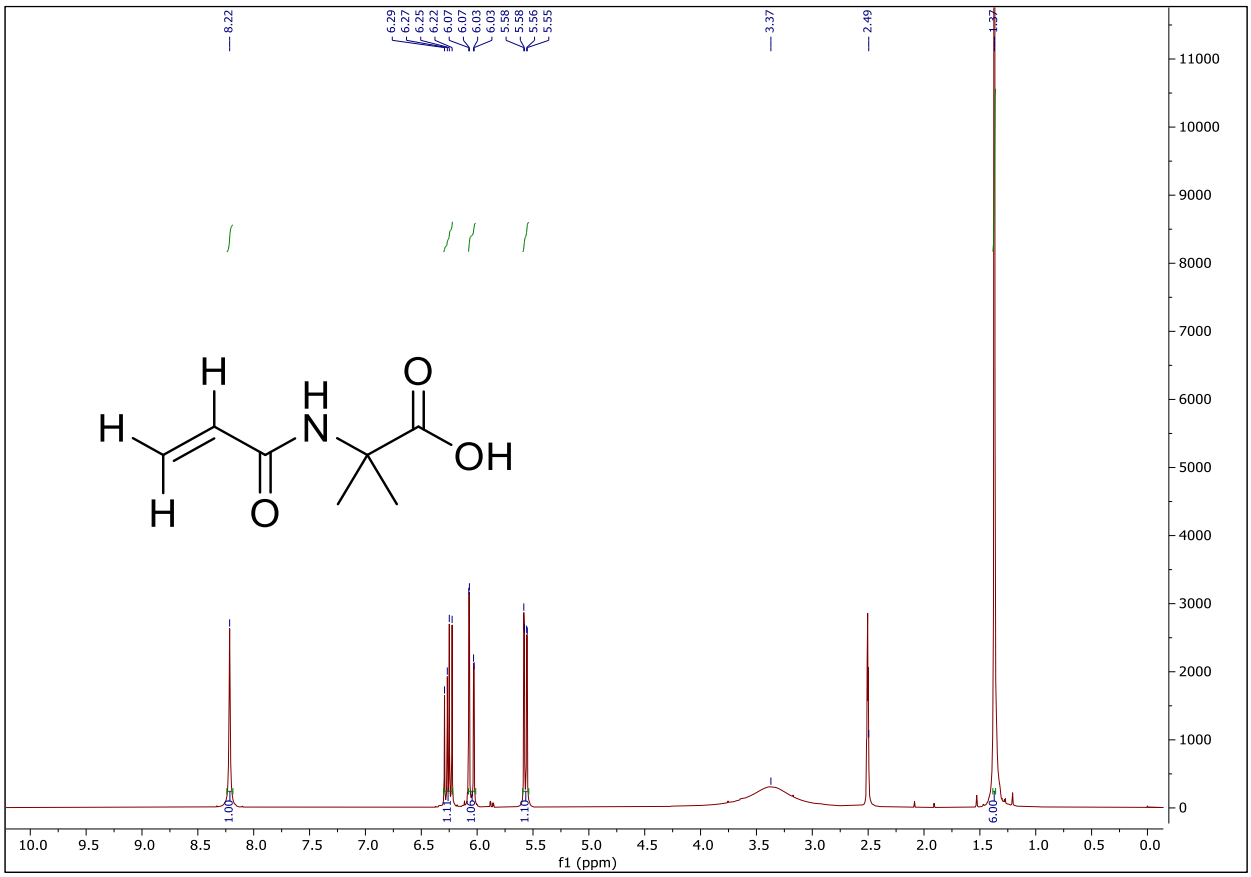

Figure S2. ^{1}H NMR spectrum (400 MHz, DMSO-d_6) of compound **1**.

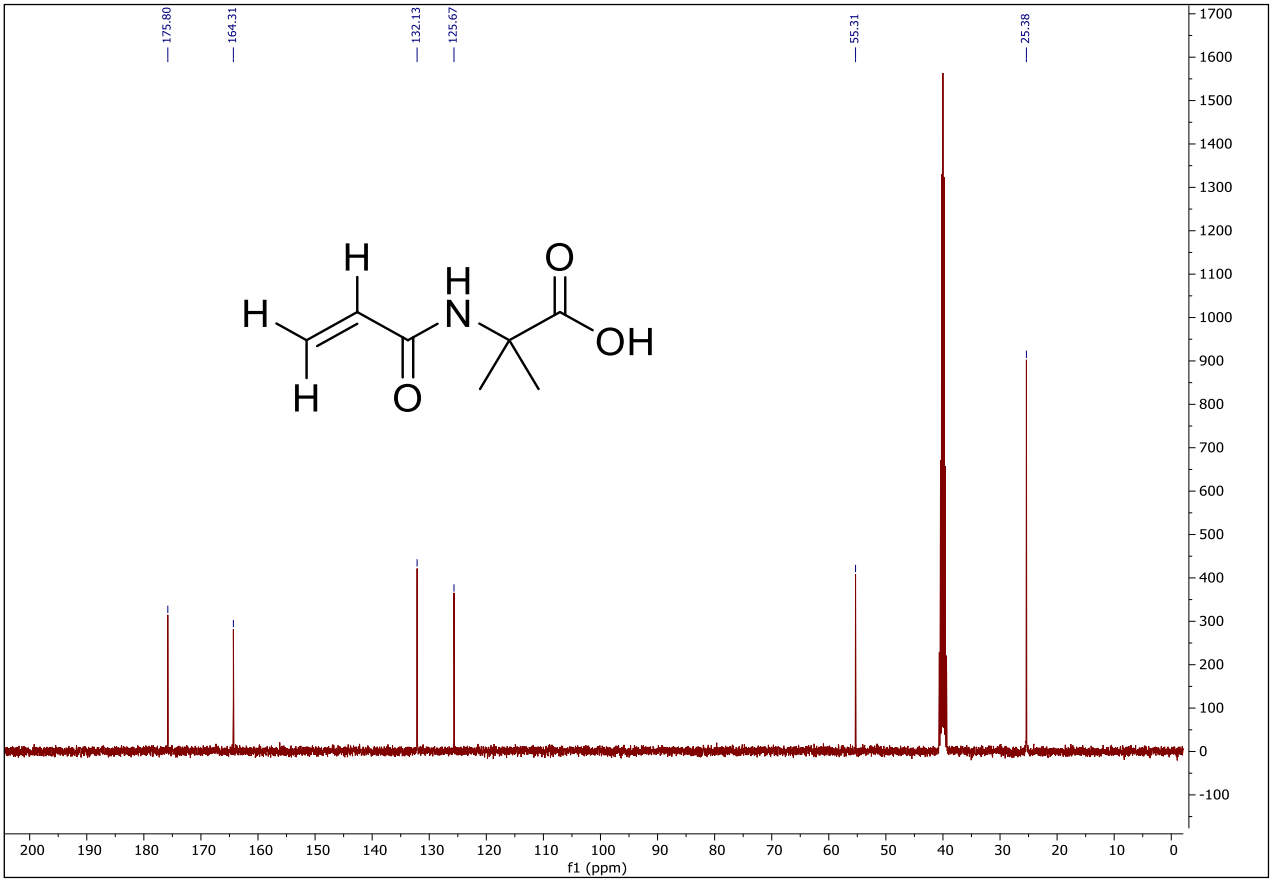

Figure S3. ^{13}C NMR spectrum (100 MHz, DMSO-d_6) of compound **1**.

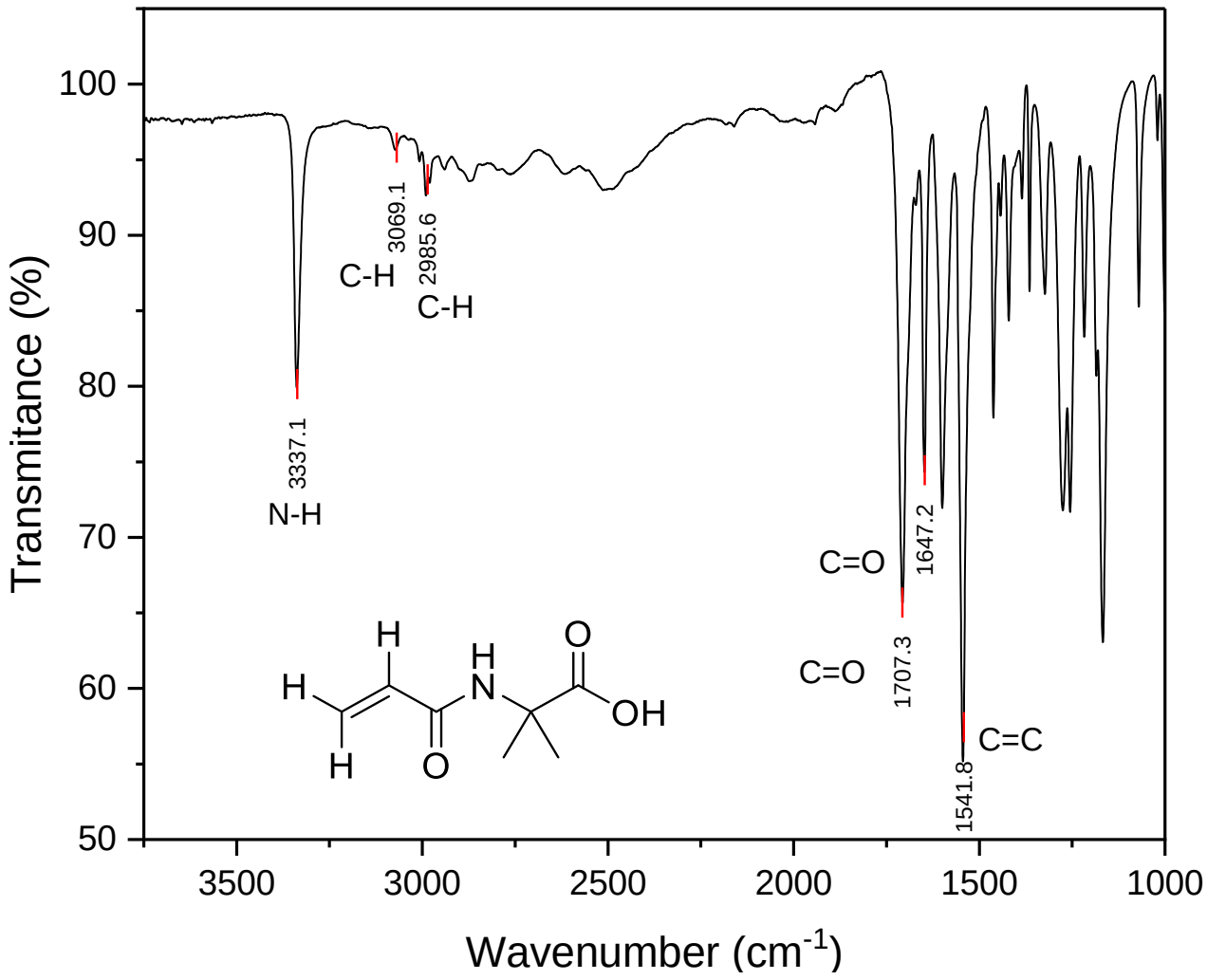

Figure S4. FTIR (KBr) spectrum of compound **1**.

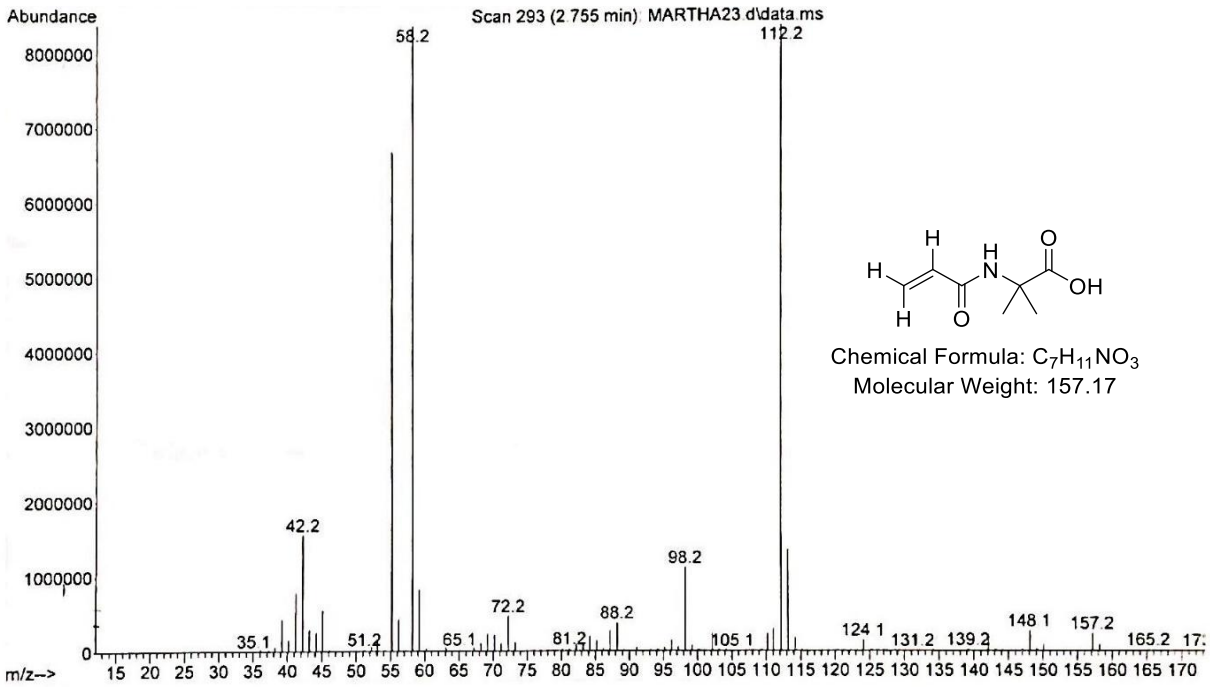

Figure S5. ESI-MS spectrum of compound **1**.

4,4-Dimethyl-2-vinyloxazol-5(4*H*)-one (VDMA)

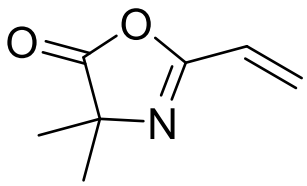

(2)

Figure S6. Structure of 4,4-dimethyl-2-vinyloxazol-5(4*H*)-one (**2**).

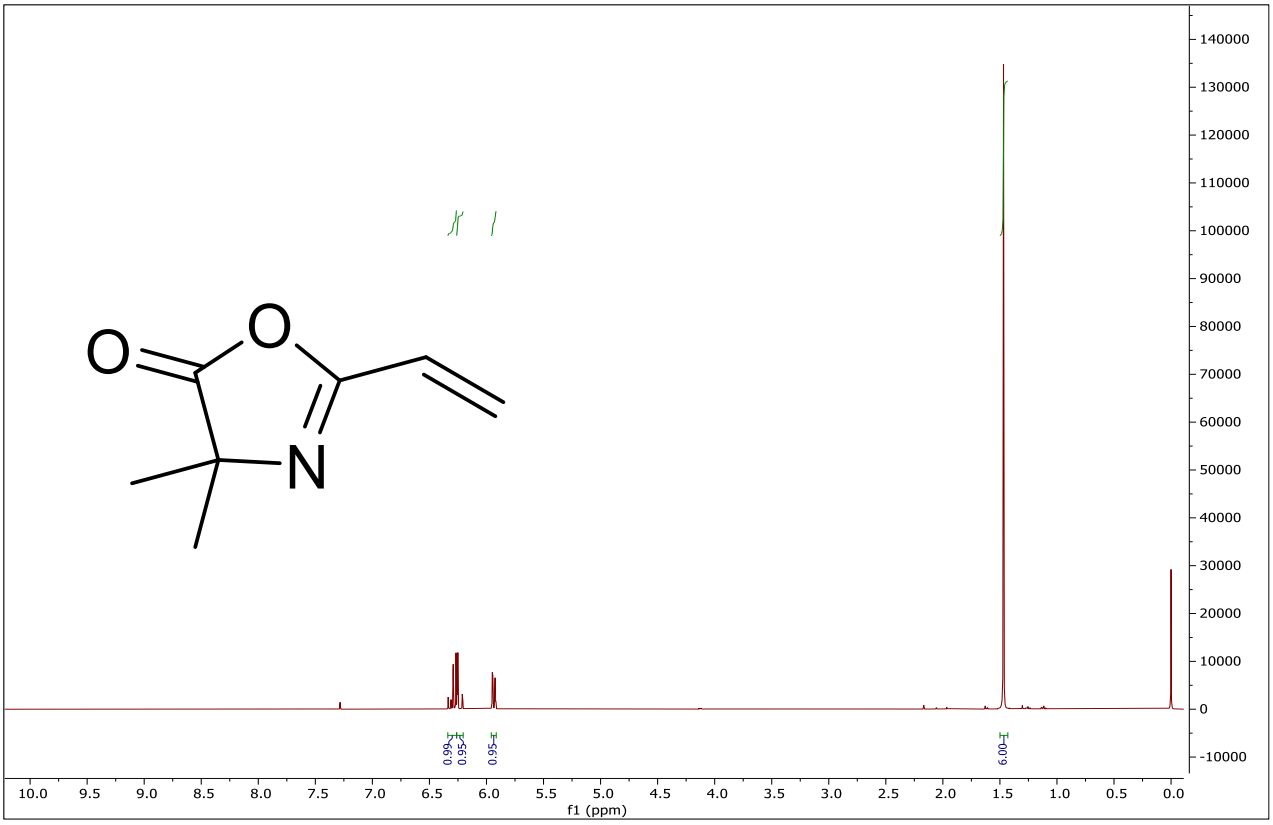

Figure S7. ^{1}H NMR (400 MHz, $CDCl_3$) spectrum of compound **2**.

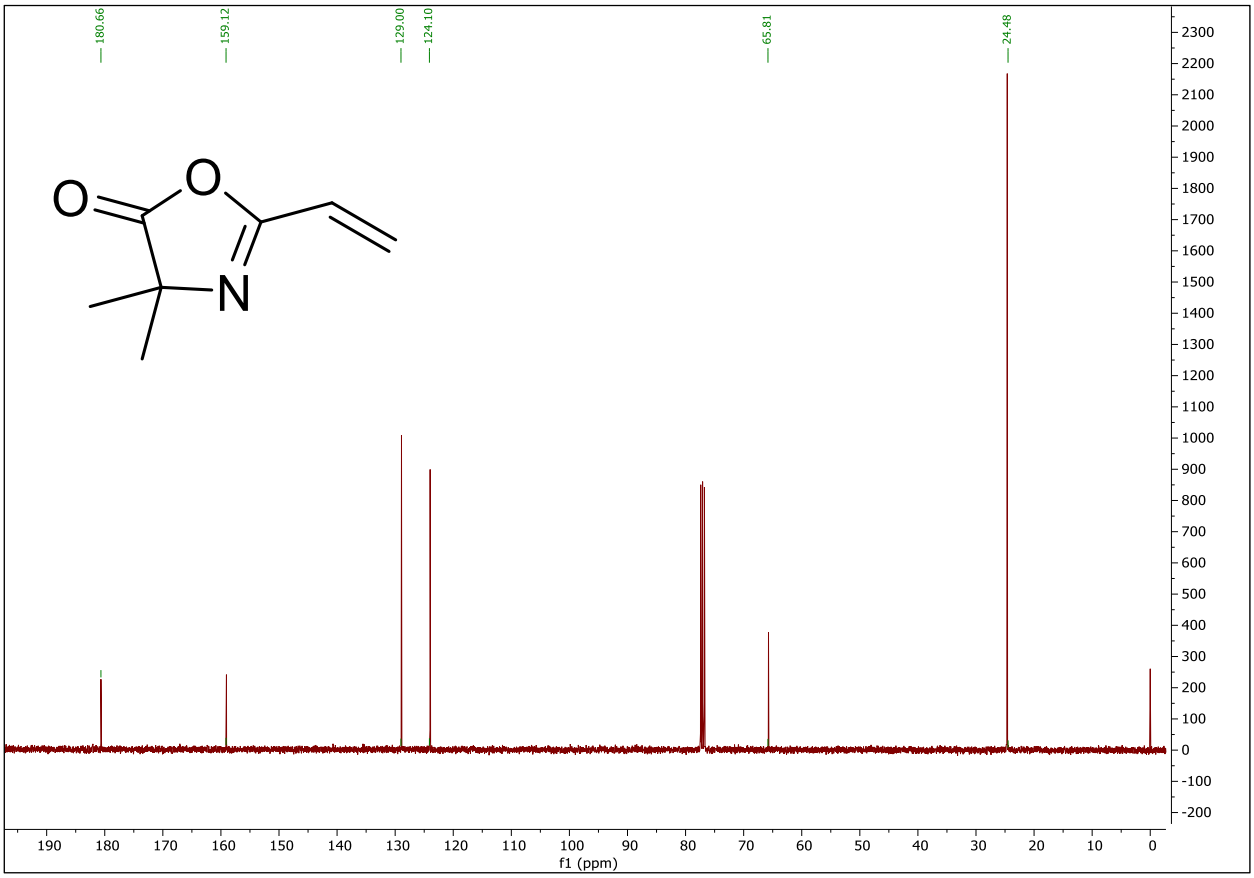

Figure S8. ^{13}C NMR (100 MHz, $CDCl_3$) spectrum of compound **2**.

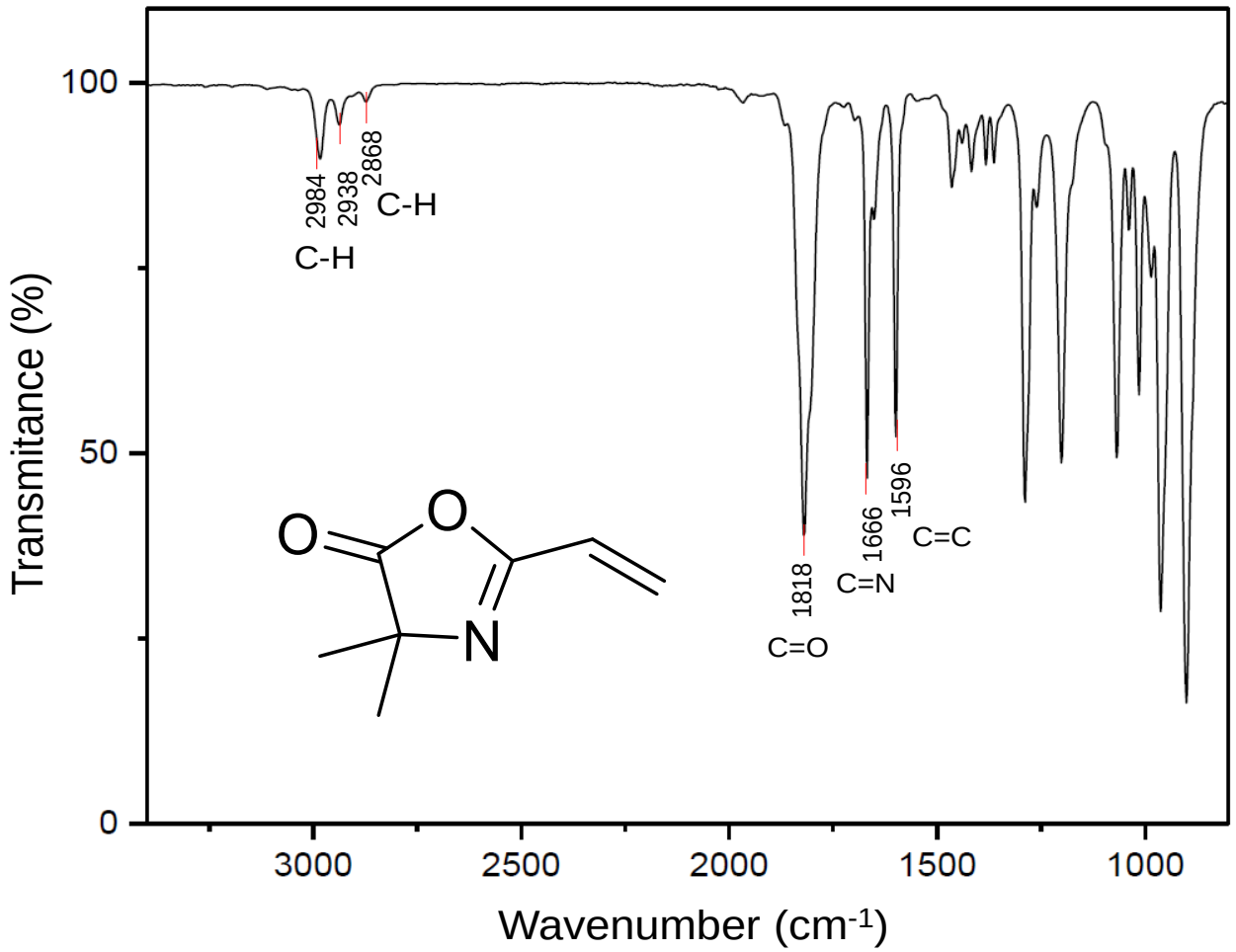

Figure S9. FTIR (KBr) spectrum of compound **2**.

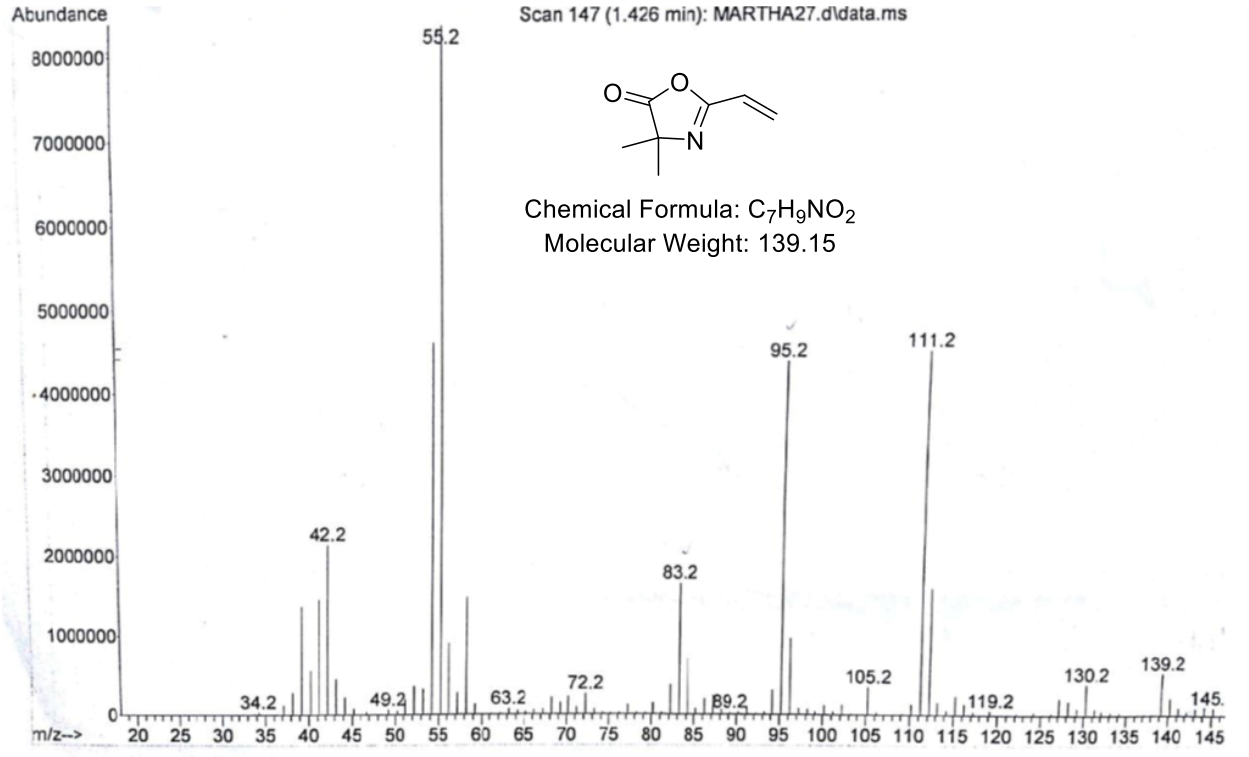

Figure S10. ESI-MS spectrum of compound **2**.

Poly(2-vinyl-4,4’-dimethylazlactone) (PVDMA)

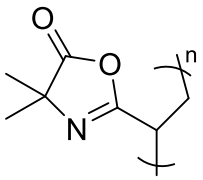

(3)

Figure S11. Structure of poly(2-vynil-4,4´-dimethylazlactone) (**3**).

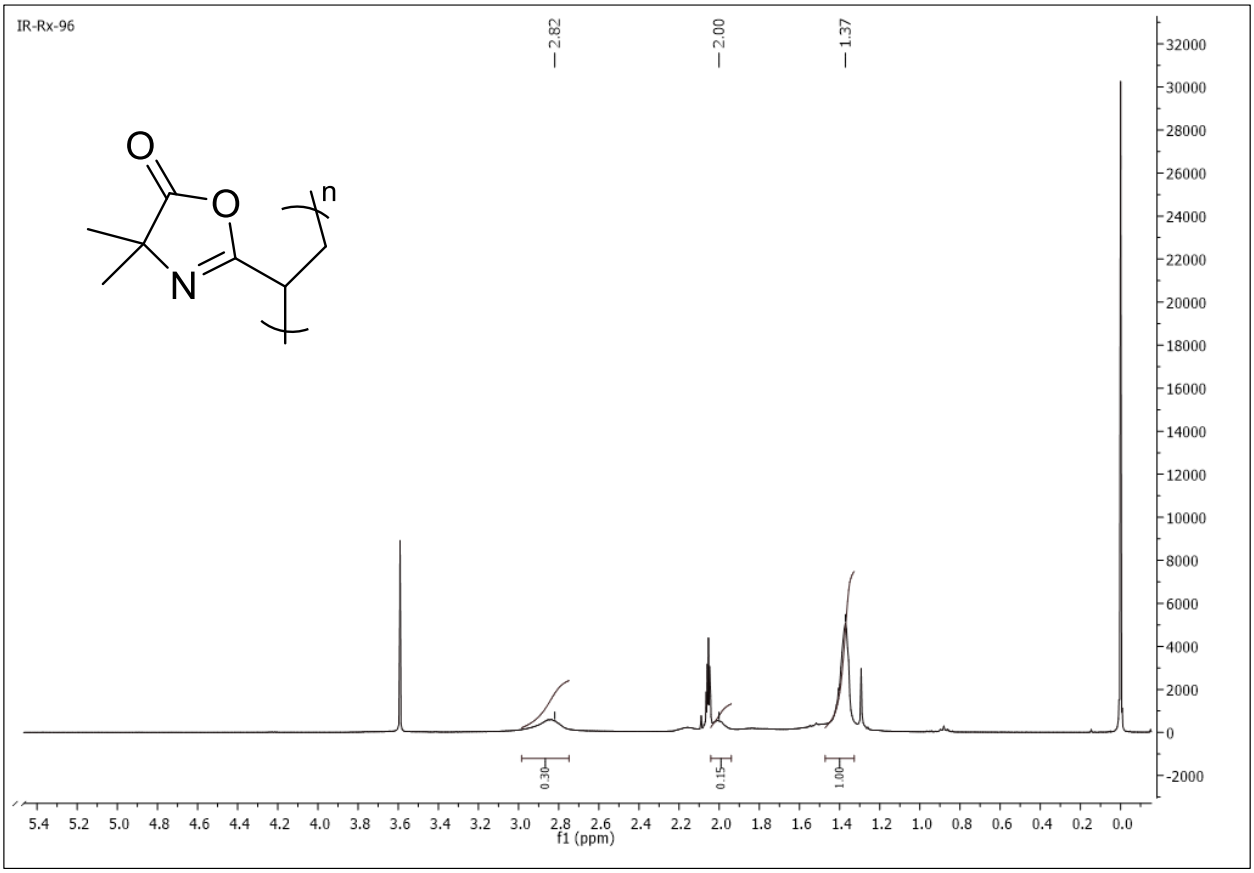

Figure S12. ^{1}H NMR (400 MHz, CD_3COCD_3) spectrum of compound **3**.

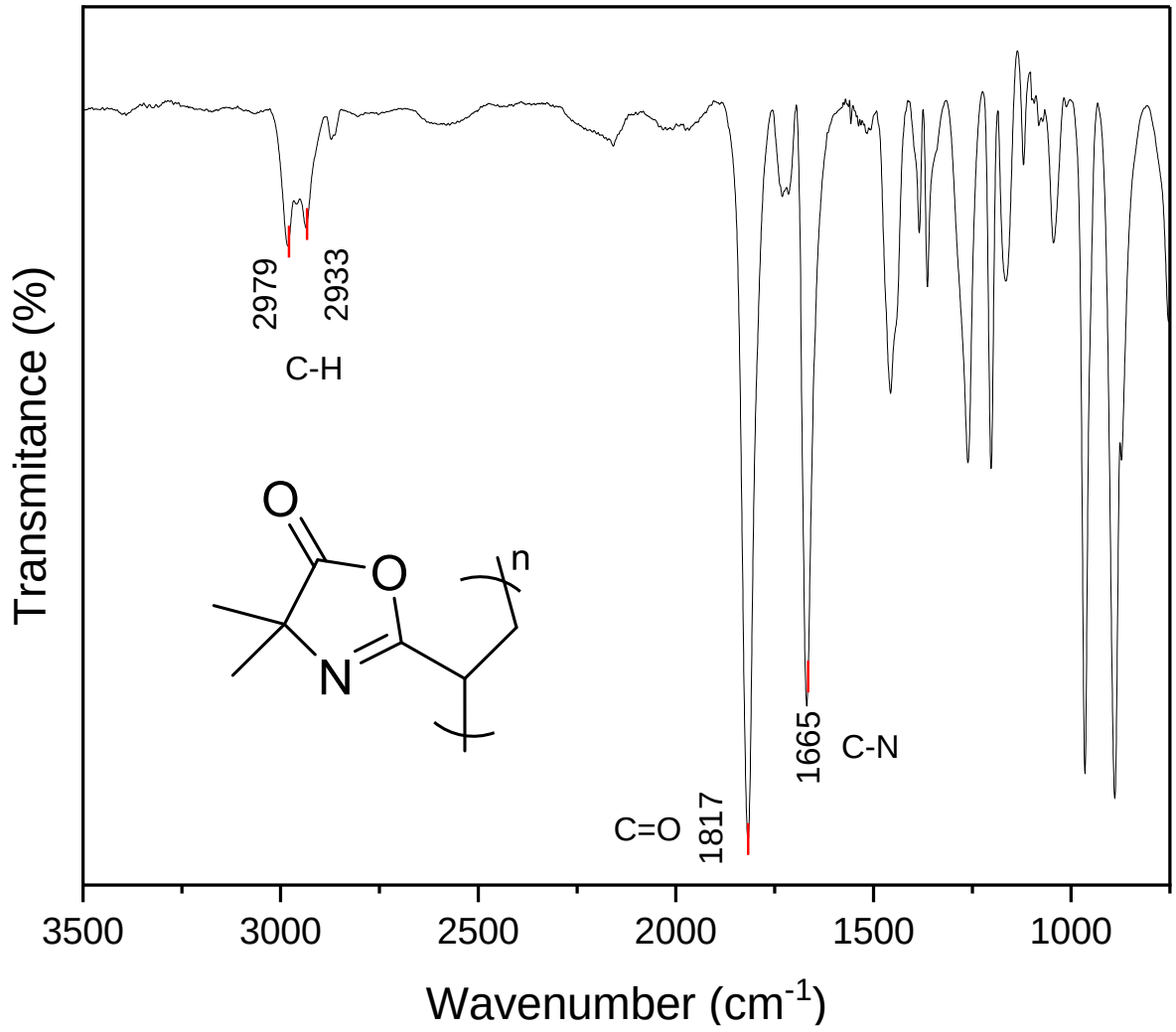

Figure S13. FTIR (KBr) spectrum of compound **3**.

Synthesis and spectroscopy of cyanine

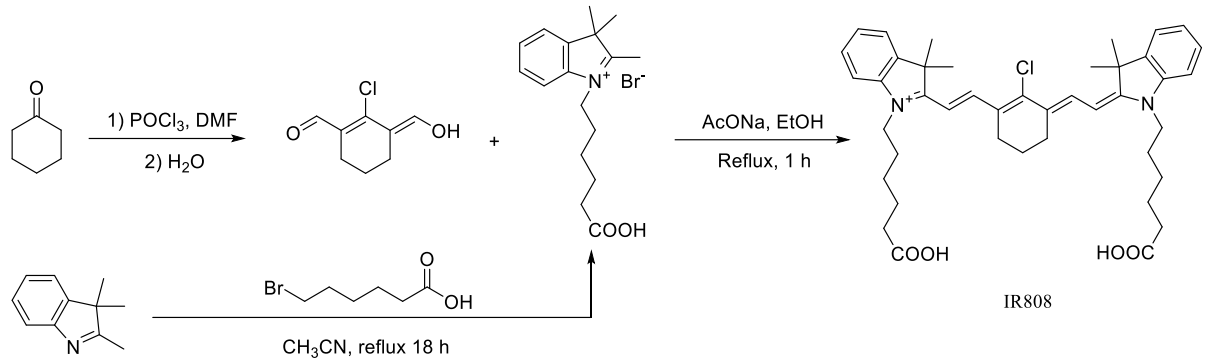

Figure S14. General synthesis route of cyanine IR808.

1-(5-Carboxypentyl)-2,3,3-trimethyl-3*H*-indol-1-ium bromide: compound **I**

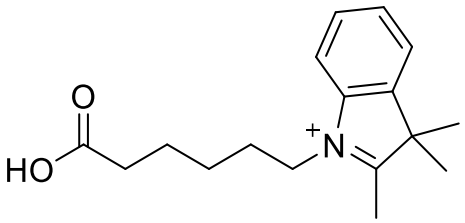

(4)

Figure S15. Structure of 1-(5-carboxypentyl)-2,3,3-trimethyl-3*H*-indol-1-ium bromide (**4**).

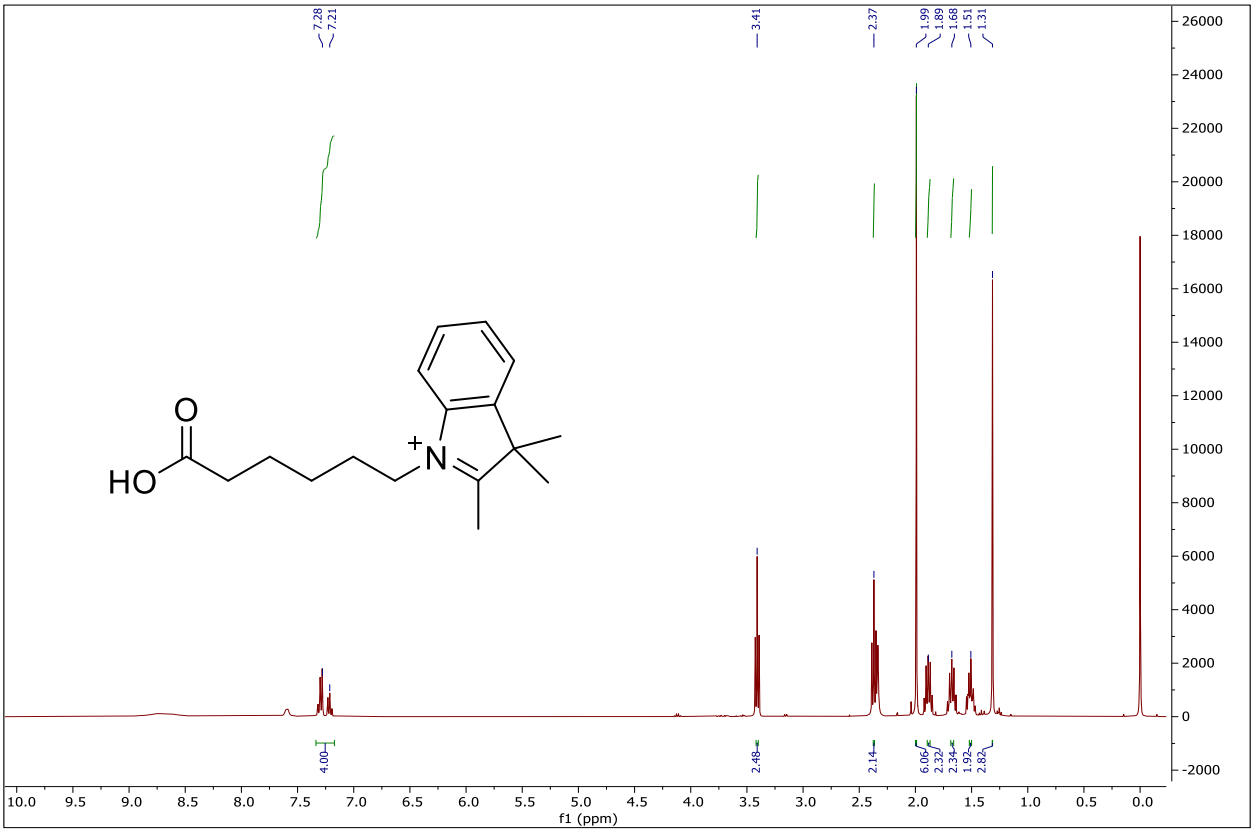

Figure S16. ^{1}H NMR (400 MHz, $CDCl_3$) spectrum of compound **4**.

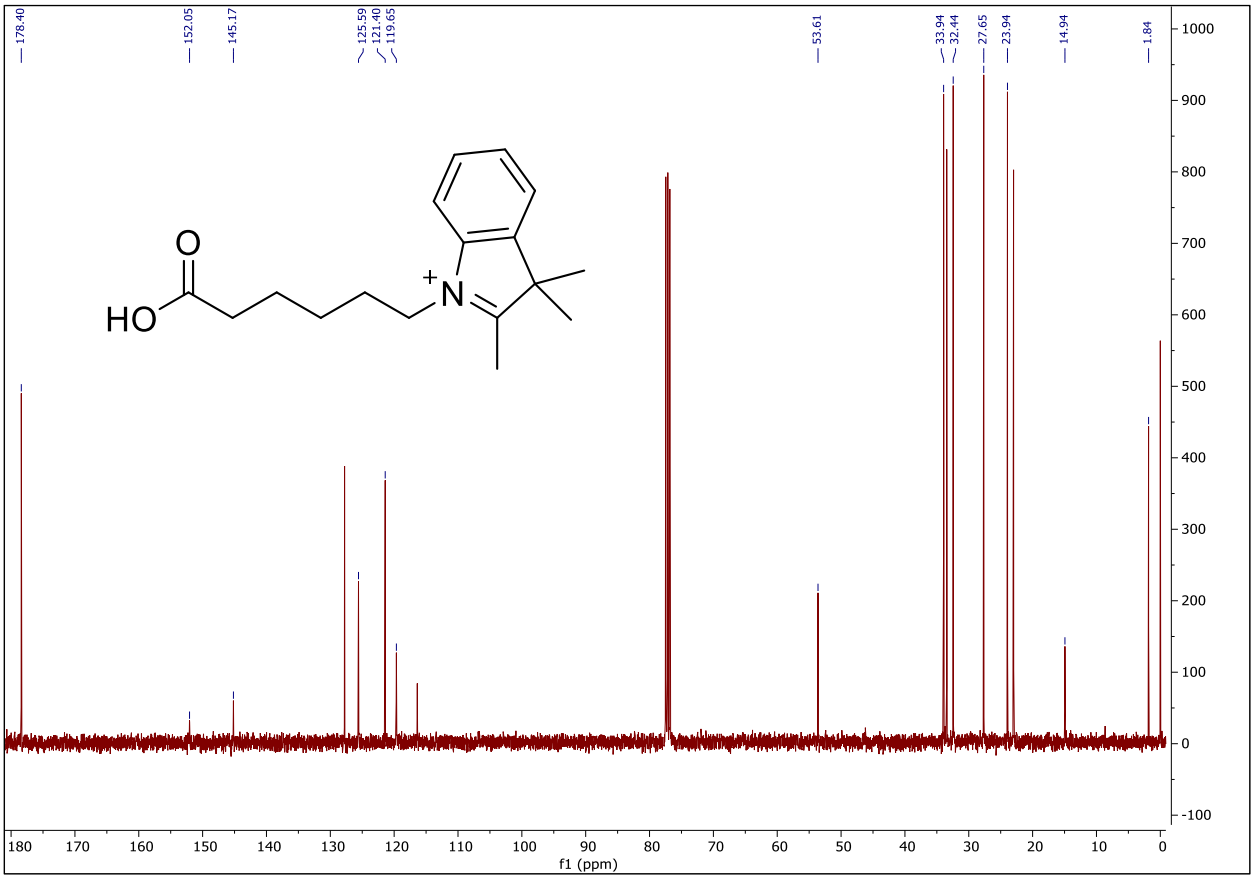

Figure S17. ^{13}C NMR (100 MHz, $CDCl_3$) spectrum of compound **4**.

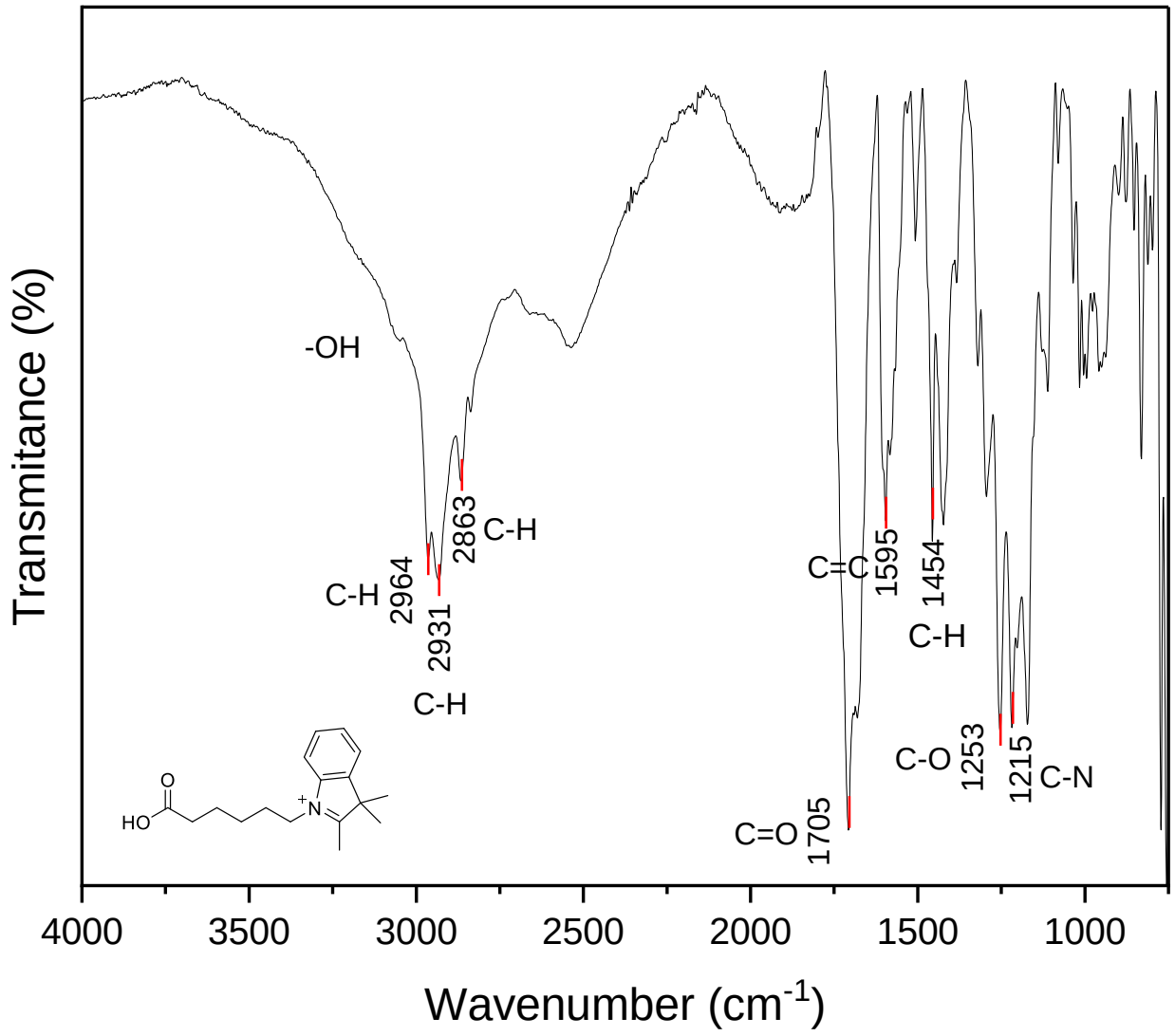

Figure S18. FTIR (KBr) spectrum of compound **4**.

(*E*)-2-Chloro-3-(hydroxymethylene)cyclohex-1-ene-1-carbaldehyde: compound **II**

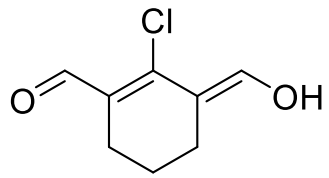

(5)

Figure S19. Structure of (*E*)-2-chloro-3-(hydroxymethylene)cyclohex-1-ene-1-carbaldehyde (**5**).

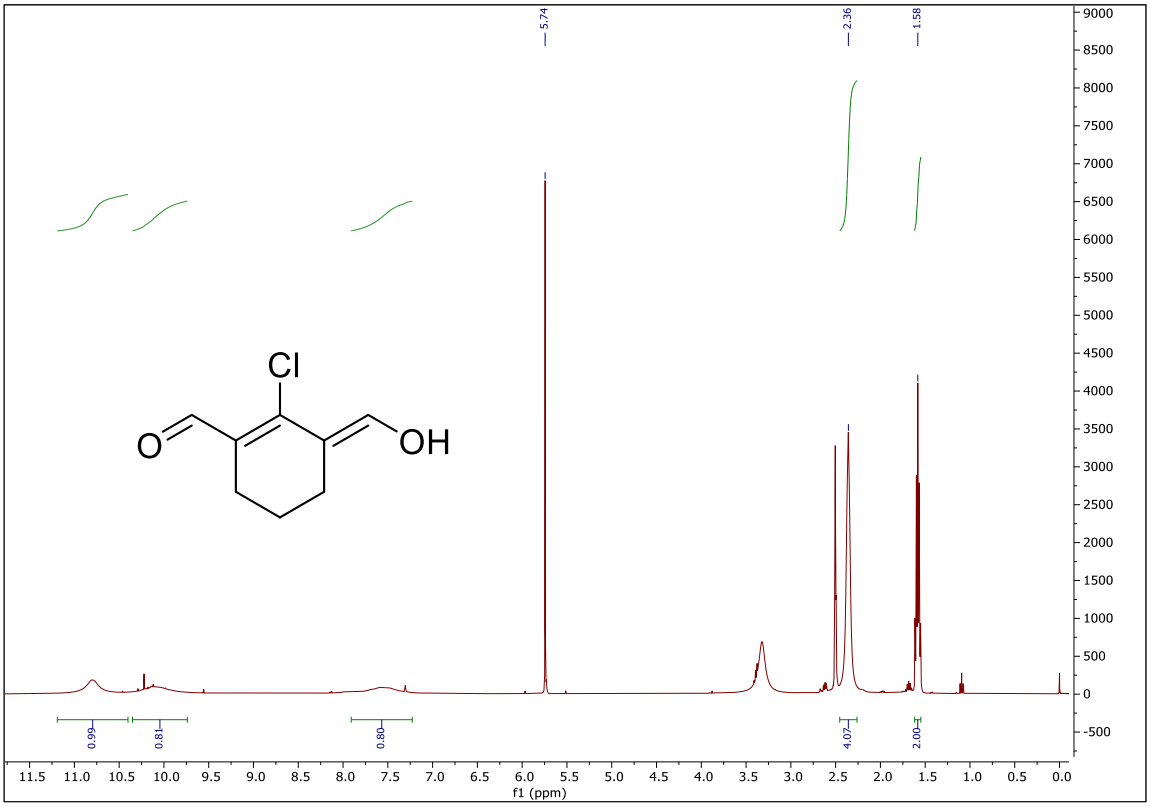

Figure S20. ^{1}H NMR (400 MHz, $CDCl_3$) spectrum of compound **5**.

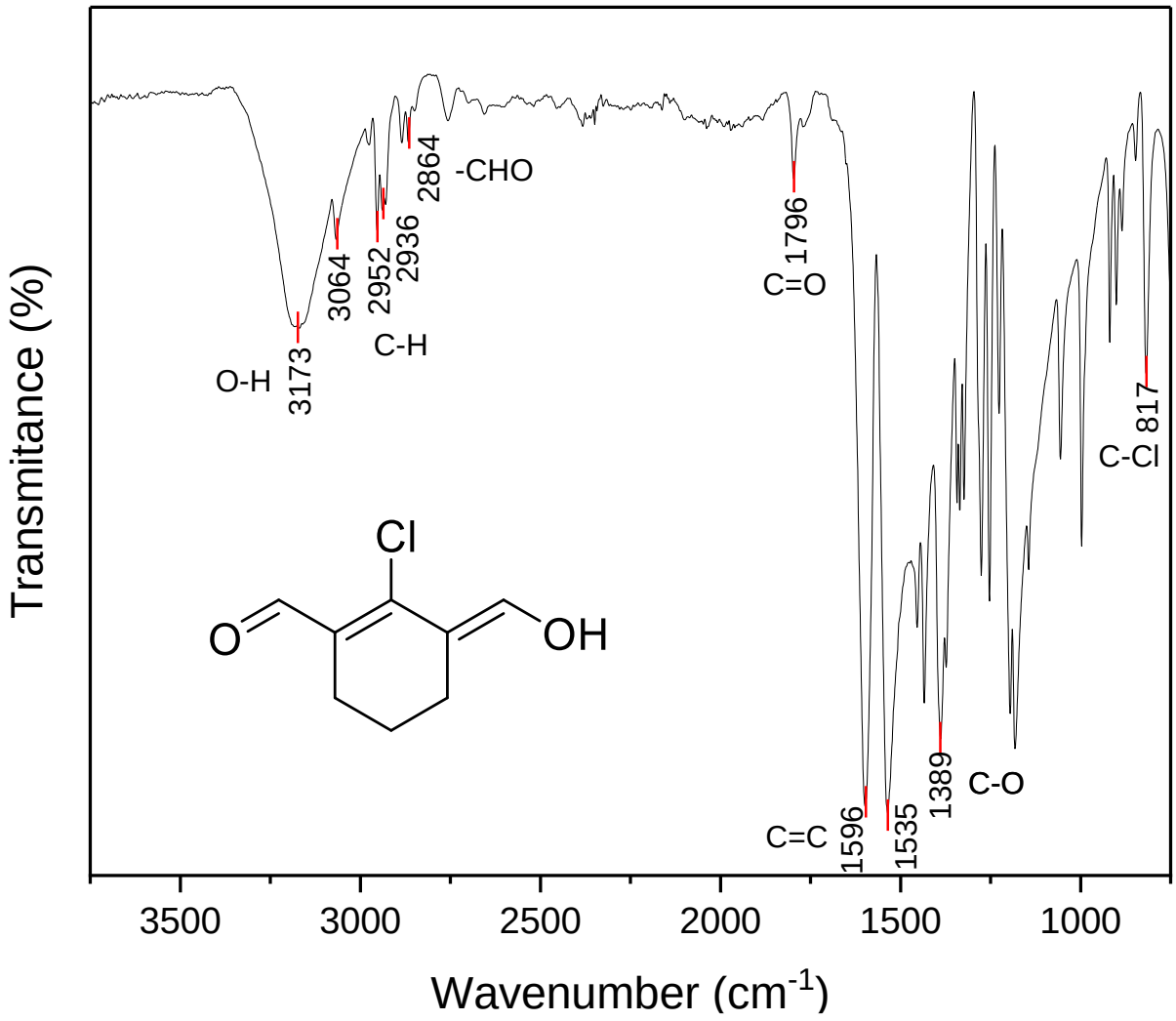

Figure S21. FTIR (KBr) spectrum of compound **5**.

Synthesis of 1-(5-carboxypentyl)-2-((*E*)-2-((*E*)-3-(2-((*E*)-1-(5-carboxypentyl)-3,3-dimethylindolin-2-ylidene)ethylidene)-2-chlorocyclohex-1-en-1-yl)vinyl)-3,3-dimethyl-3H-indol-1-ium: IR808

(6)

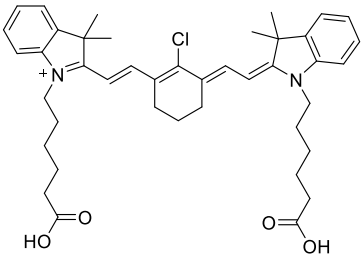

Figure S22. Structure of IR808 (**6**).

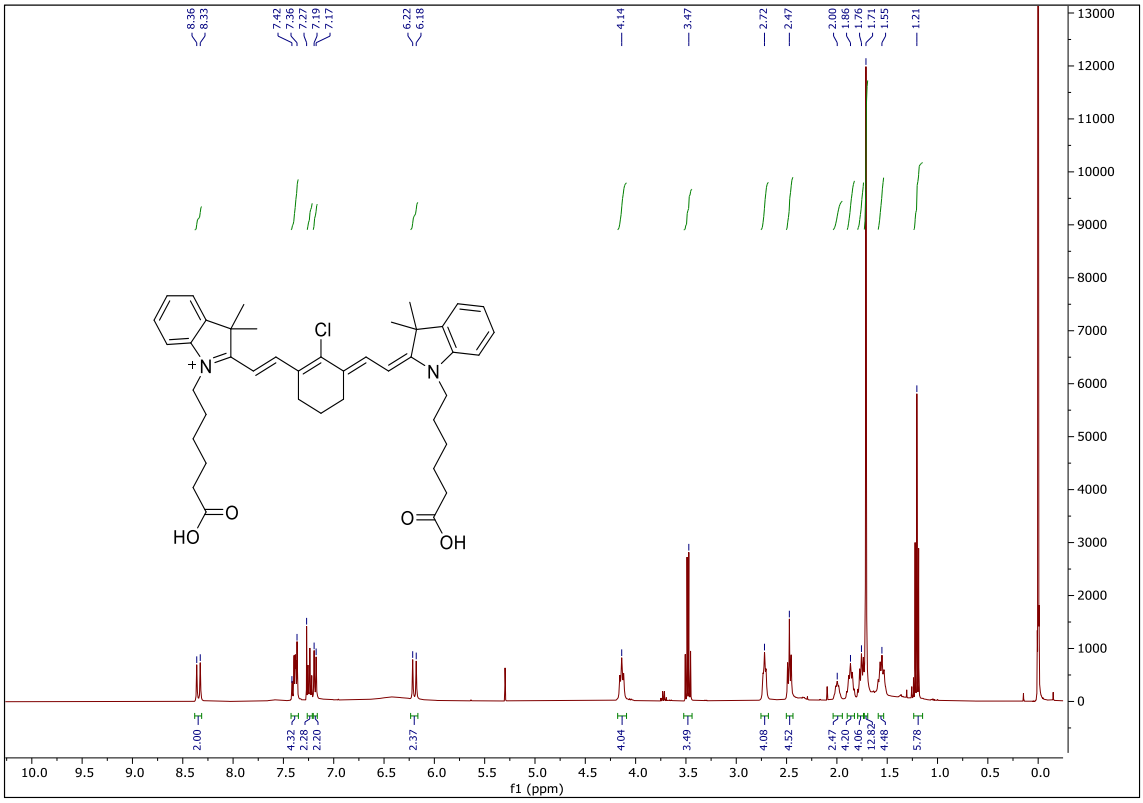

Figure S23. ^{1}H NMR (400 MHz, $CDCl_3$) spectrum of compound **6**.

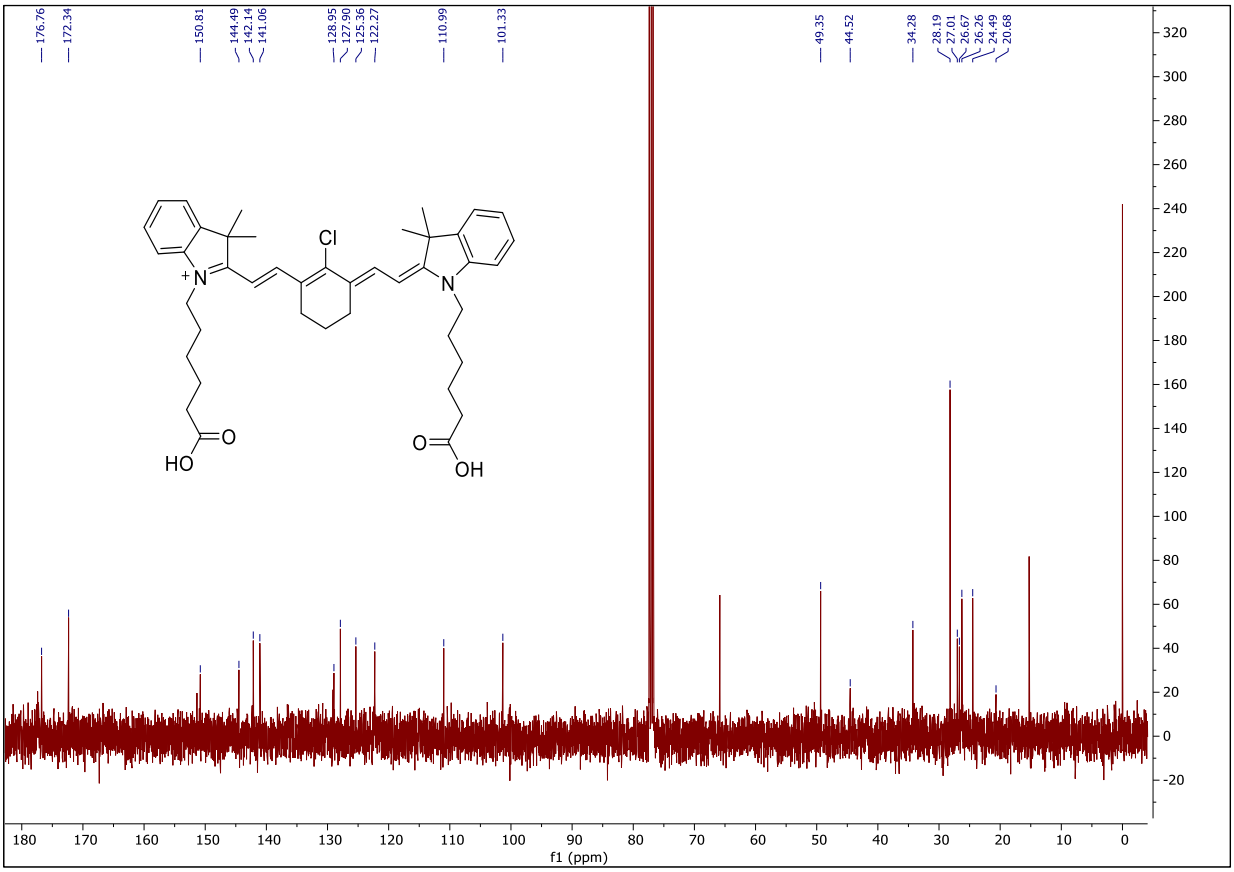

Figure S24. ^{13}C NMR (100 MHz, $CDCl_3$) spectrum of compound **6**.

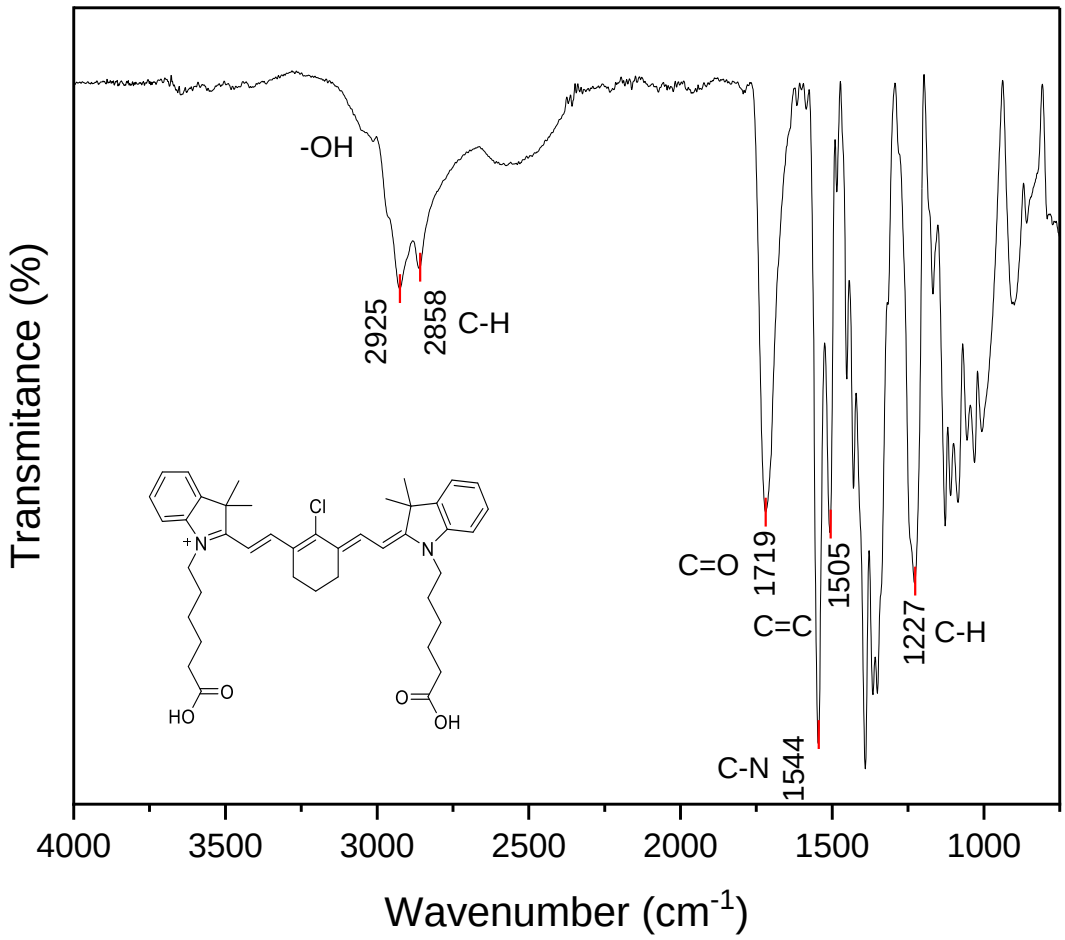

Figure S25. FTIR (KBr) spectrum of compound **6**.

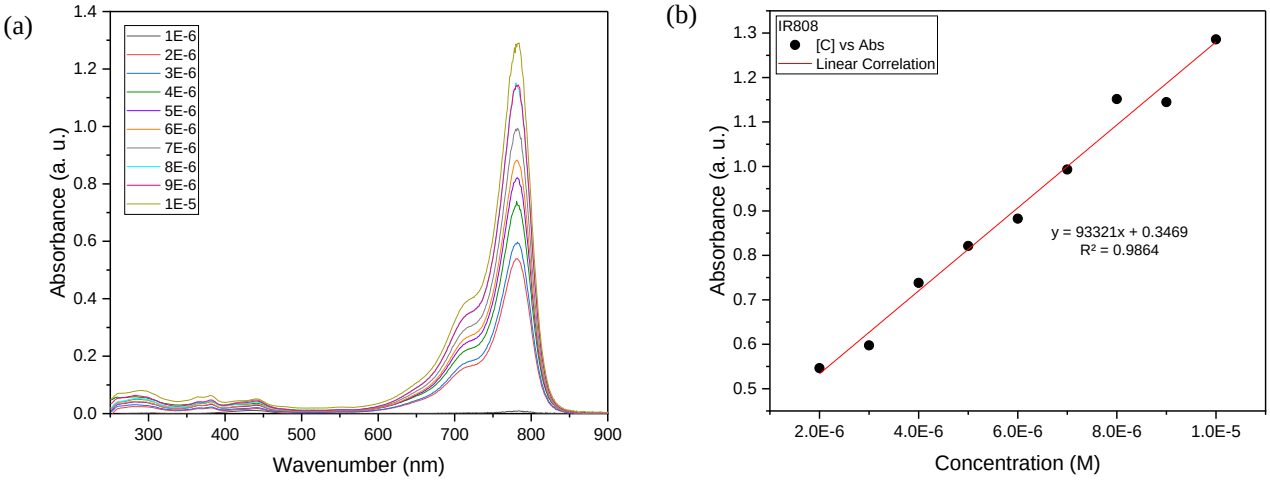

Figure S26. Spectroscopic analysis of compound **6**. (a) UV-Vis spectroscopy and (b) calibration curve.

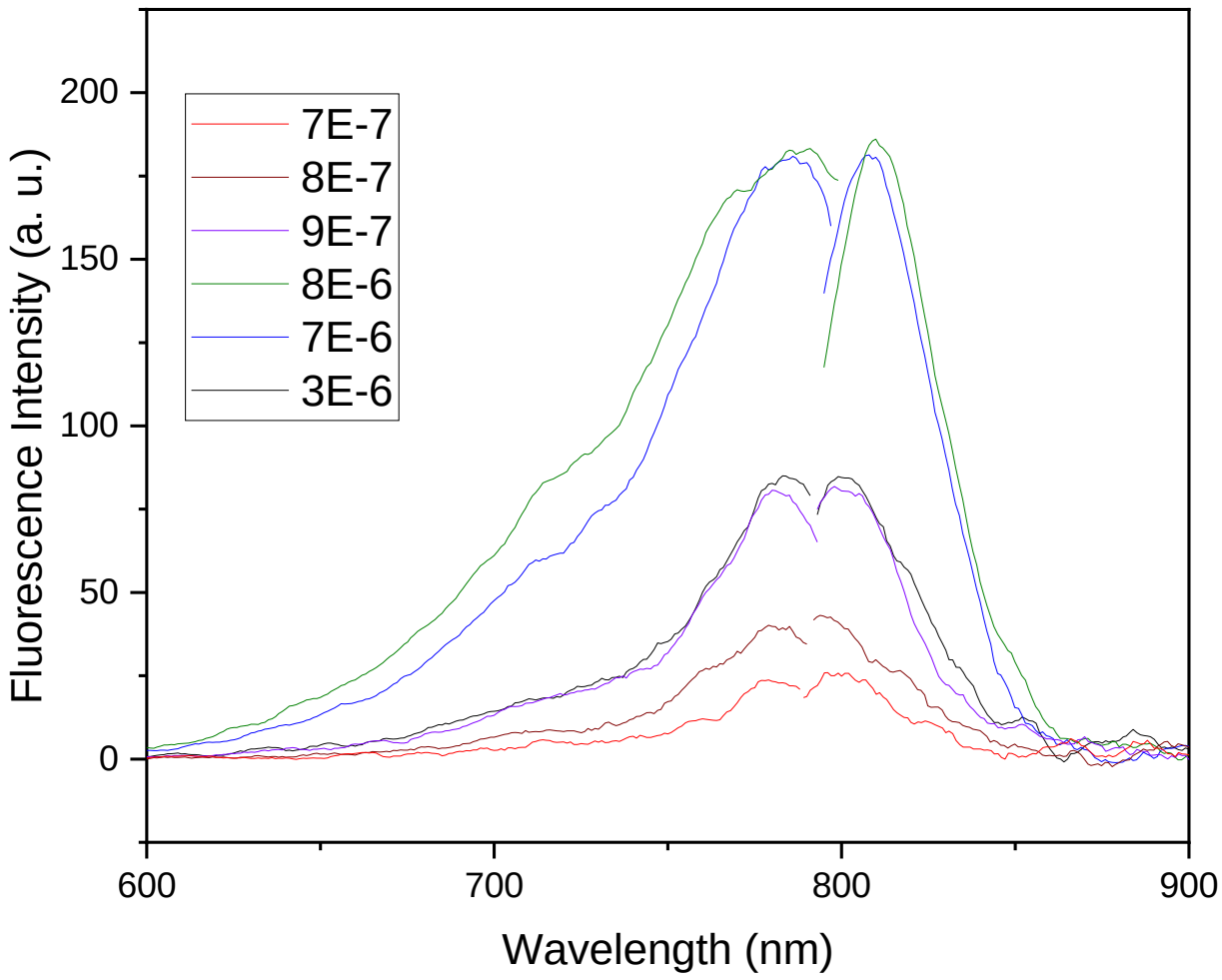

Figure S27. Fluorescence spectrum of compound **6**.

To quantify the fluorescence quantum yield (ϕ), the comparative slope method was used. This involved constructing a graph of integrated fluorescence intensity as a function of absorbance measured at the corresponding wavelength. The comparison was performed using IR780 as the standard, which has a known quantum yield of 0.17 when measured in EtOH, and the synthesized cyanine. Figure S28 shows the linear relationships with an R^2 greater than 0.98 for both compounds, yielding slope values of 11595.9 and 54195 for IR780 and IR808, respectively. The following formula was applied using these values:

$$\phi_f = \frac{\phi_{f,\,Ref} \cdot m_f \cdot n^2}{m_{f,\,Ref} \cdot n_{Ref}^2} = 0.355 \quad \text{(S1)}$$

where:

ϕ_f: quantum yield (sample)

$\phi_{f,\,Ref}$: quantum yield (reference), 0.17

m_f: slope sample (5419.5)

$m_{f,\,Ref}$: slope reference (11595.9)

n: refractive index of the sample solvent (ACN: 1.34)

n_{Ref}: refractive index of the reference solvent (EtOH: 1.36)

Substituting the values into the formula yielded a quantum yield of 0.36 for the cyanine under study.

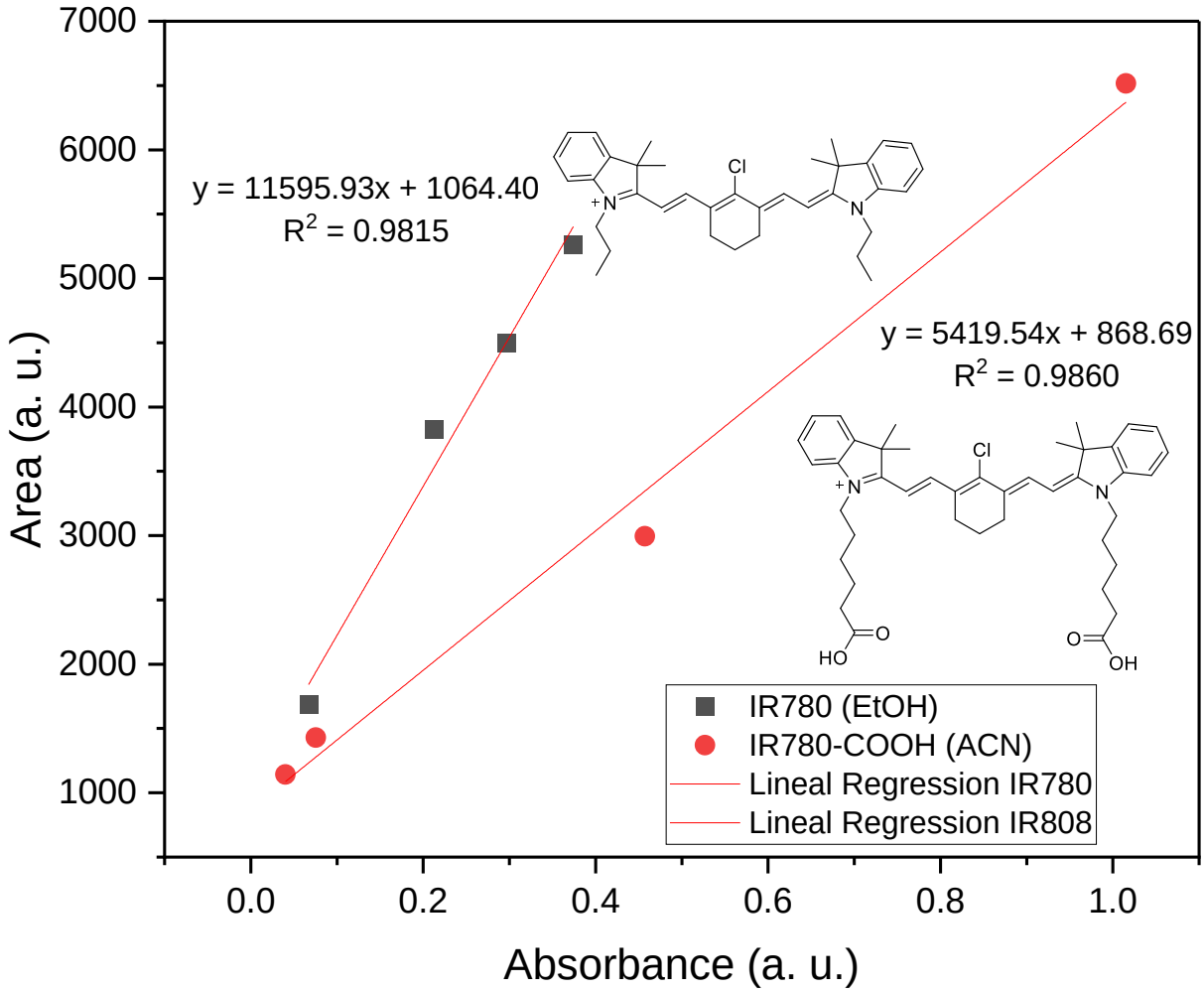

Figure S28. Comparative graph of the fluorescent response of compound **6** and synthesized cyanine as a function of absorbance.

AFM characterization of PVDMA/PEI films

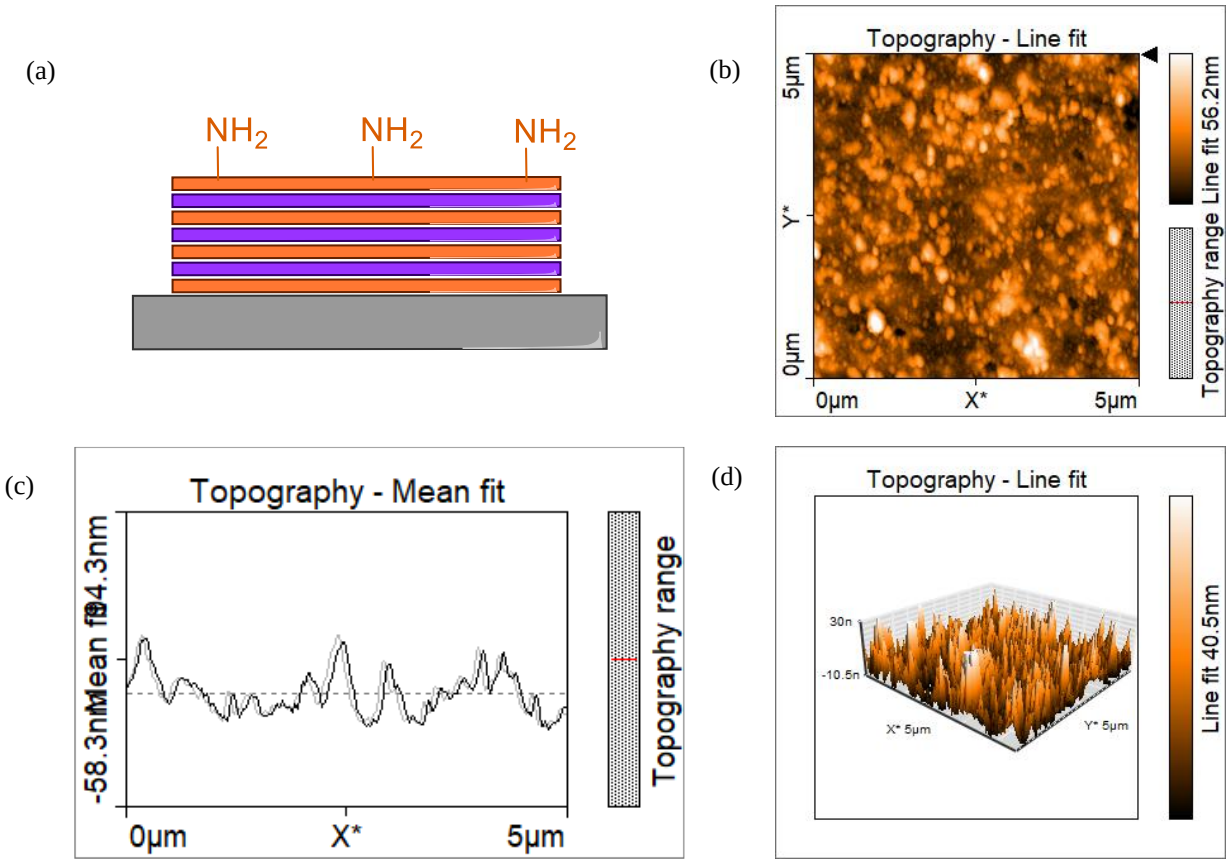

Figure S29. Characterization of the reactive PVDMA/PEI film with 15.5 bilayers by AFM: (a) schematic representation, (b) 2D image of surface topography, (c) topographic profile, (d) 3D surface reconstruction.

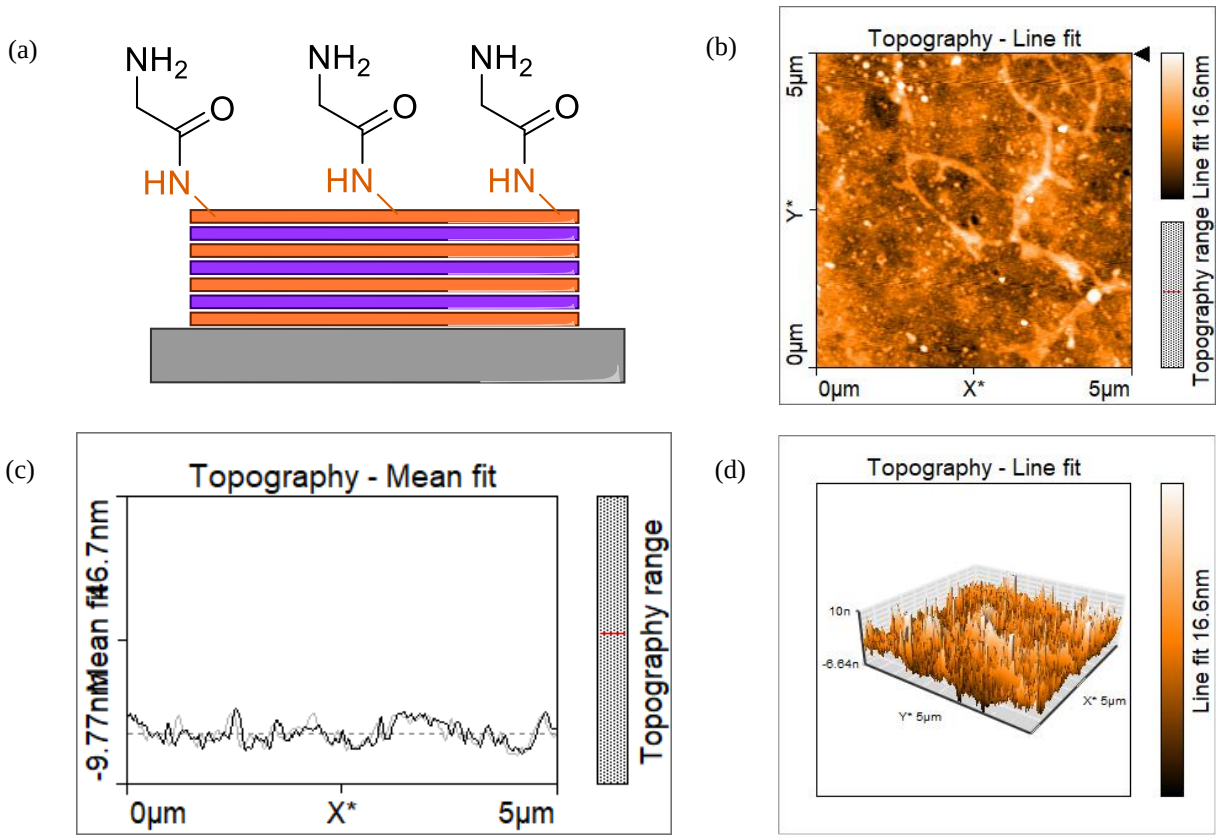

Figure S30. Characterization of the reactive PVDMA/PEI-Gly with 15.5 bilayers by AFM: (a) schematic representation, (b) 2D image of surface topography, (c) topographic profile, (d) 3D surface reconstruction.

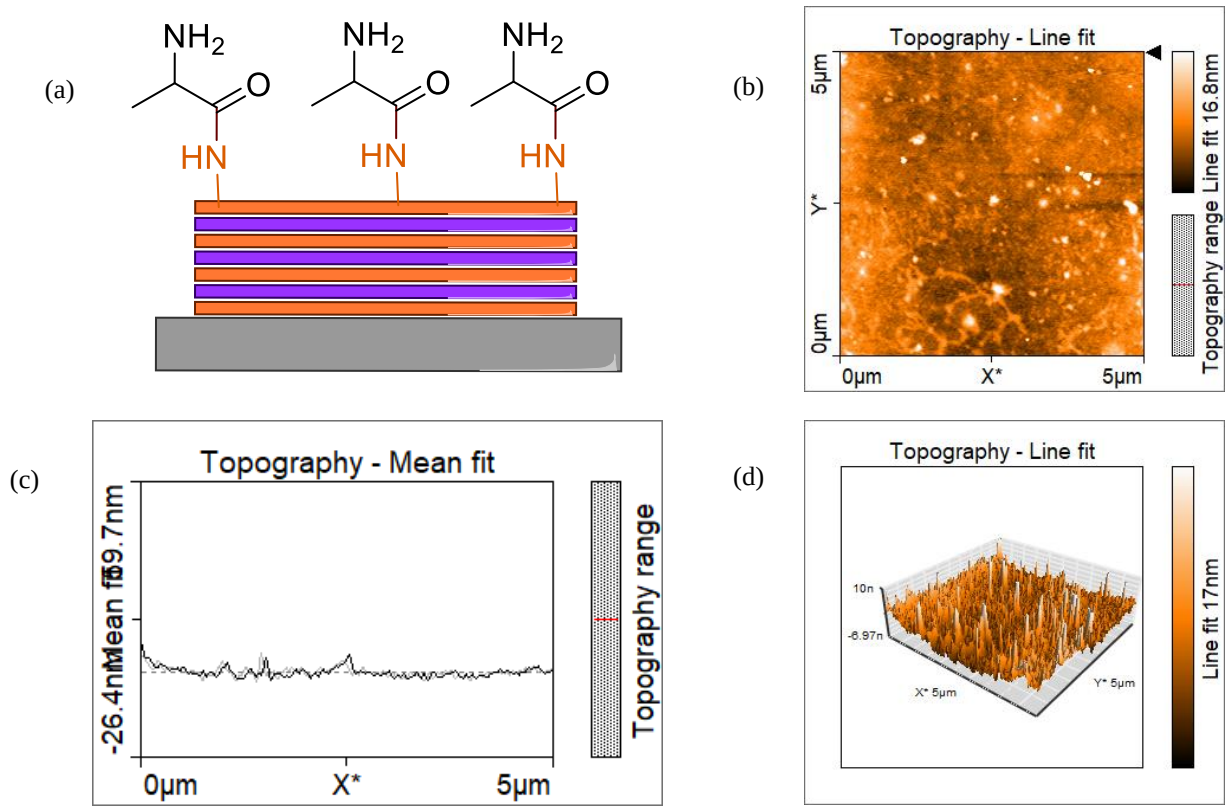

Figure S31. Characterization of the reactive PVDMA/PEI-Ala with 15.5 bilayers by AFM: (a) schematic representation, (b) 2D image of surface topography, (c) topographic profile, (d) 3D surface reconstruction.

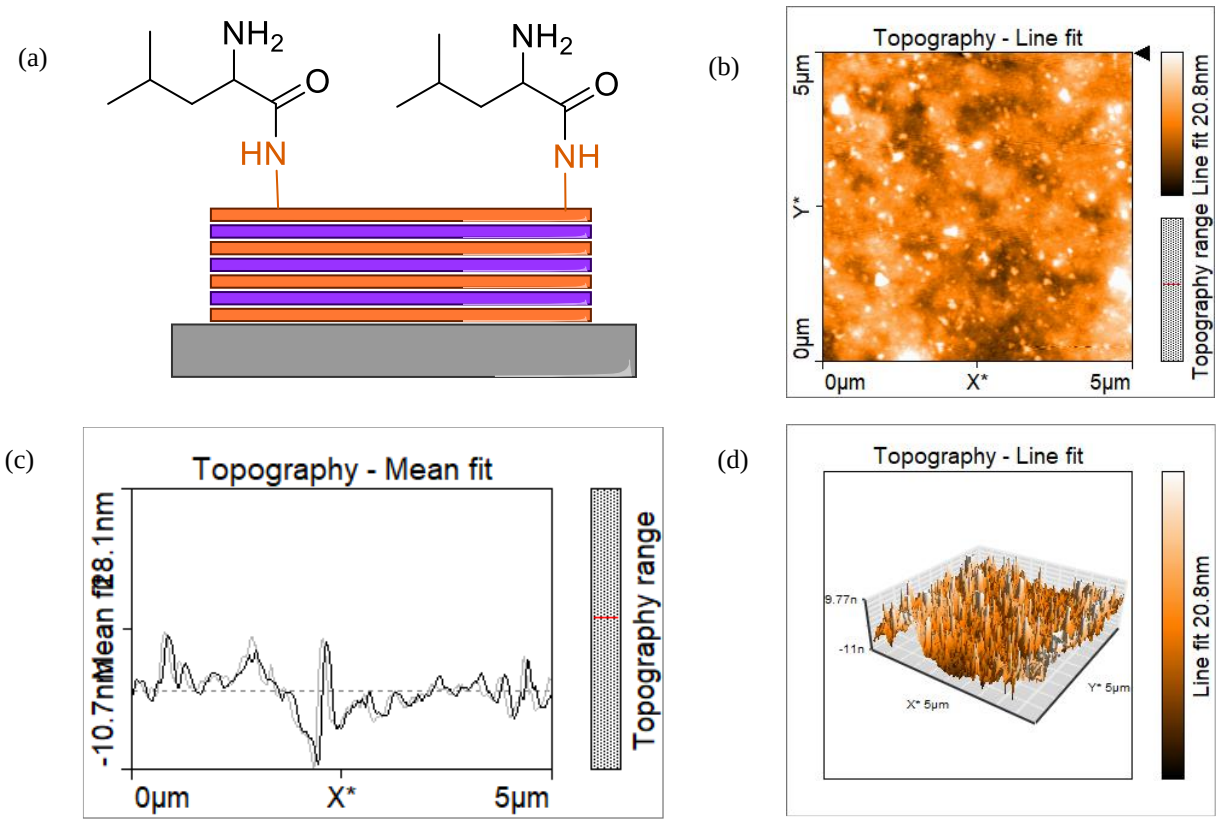

Figure S32. Characterization of the reactive PVDMA/PEI-Leu with 15.5 bilayers by AFM: (a) schematic representation, (b) 2D image of surface topography, (c) topographic profile, (d) 3D surface reconstruction.

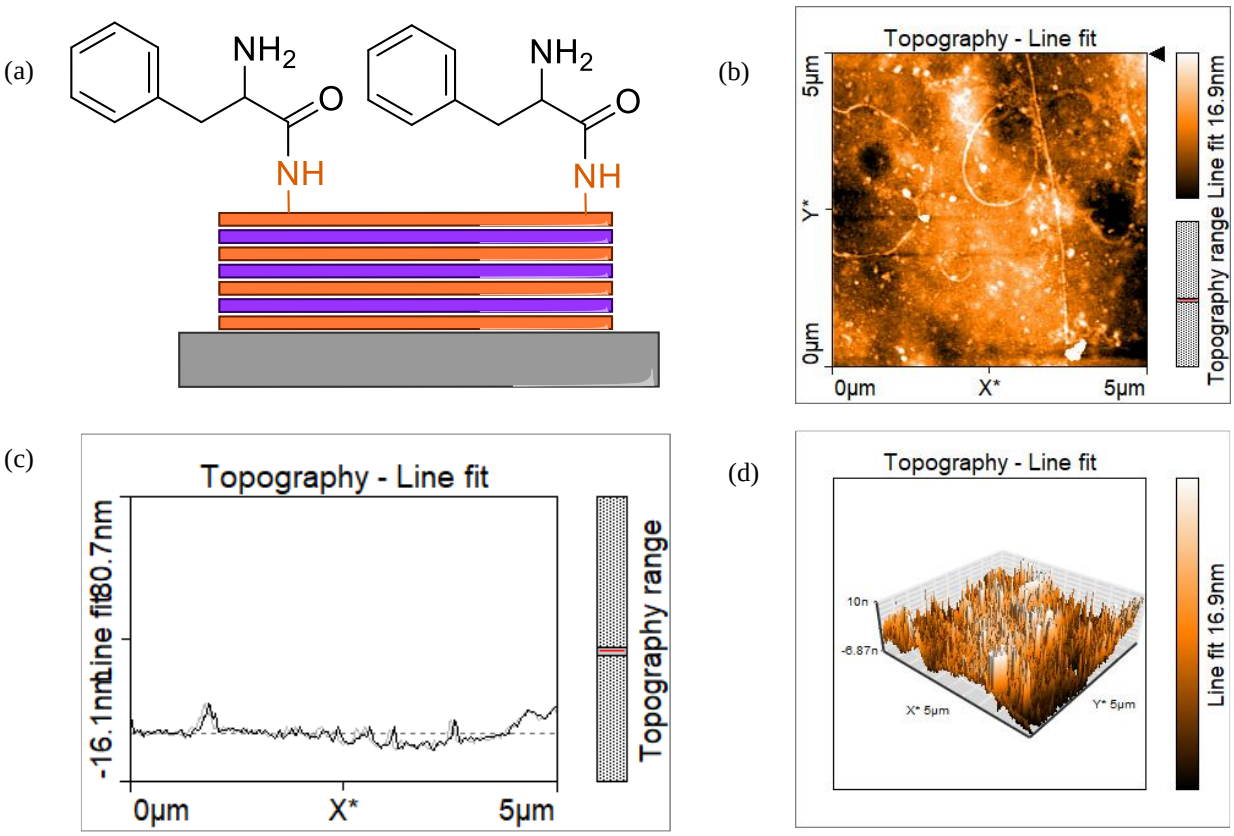

Figure S33. Characterization of the reactive PVDMA/PEI-Phe with 15.5 bilayers by AFM: (a) schematic representation, (b) 2D image of surface topography, (c) topographic profile, (d) 3D surface reconstruction.

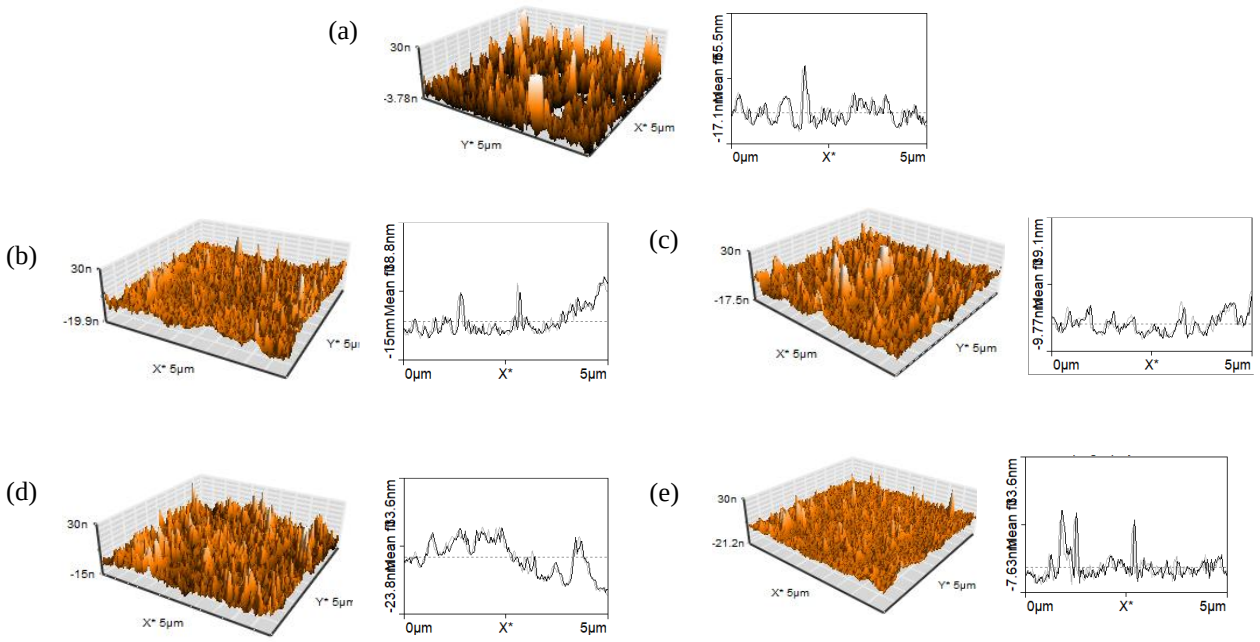

Figure S34. Atomic force microscopy (AFM) analysis of (a) unfunctionalized 15.5-bilayer PVDMA/PEI film (terminal amines) and films functionalized with (b) Fmoc-Gly, (c) Fmoc-Ala, (d) Fmoc-Leu and E) Fmoc-Phe.

General characterization of PVDMA/PEI films

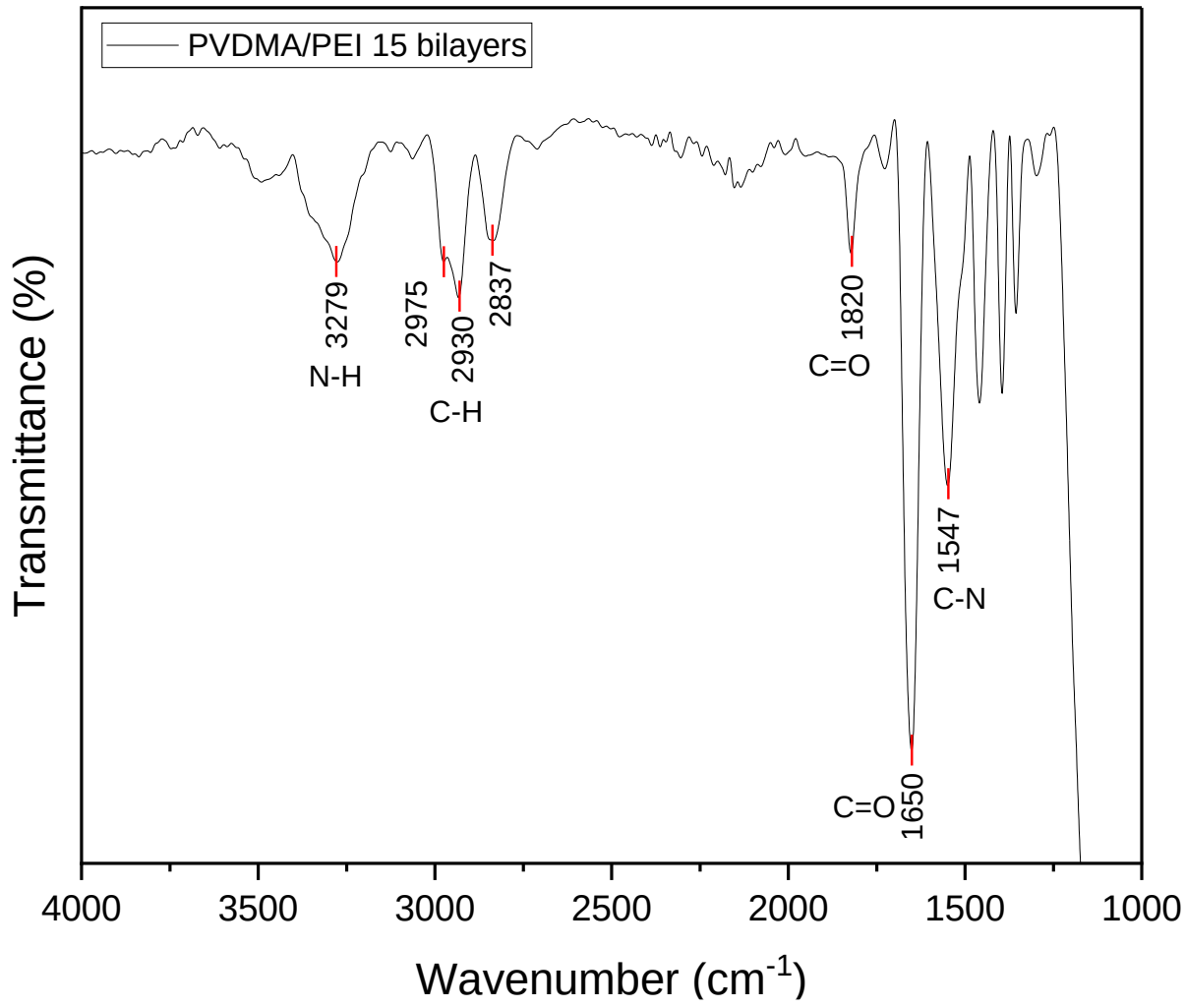

Figure S35. FTIR (KBr) spectrum of 15 bilayer PVDMA/PEI.

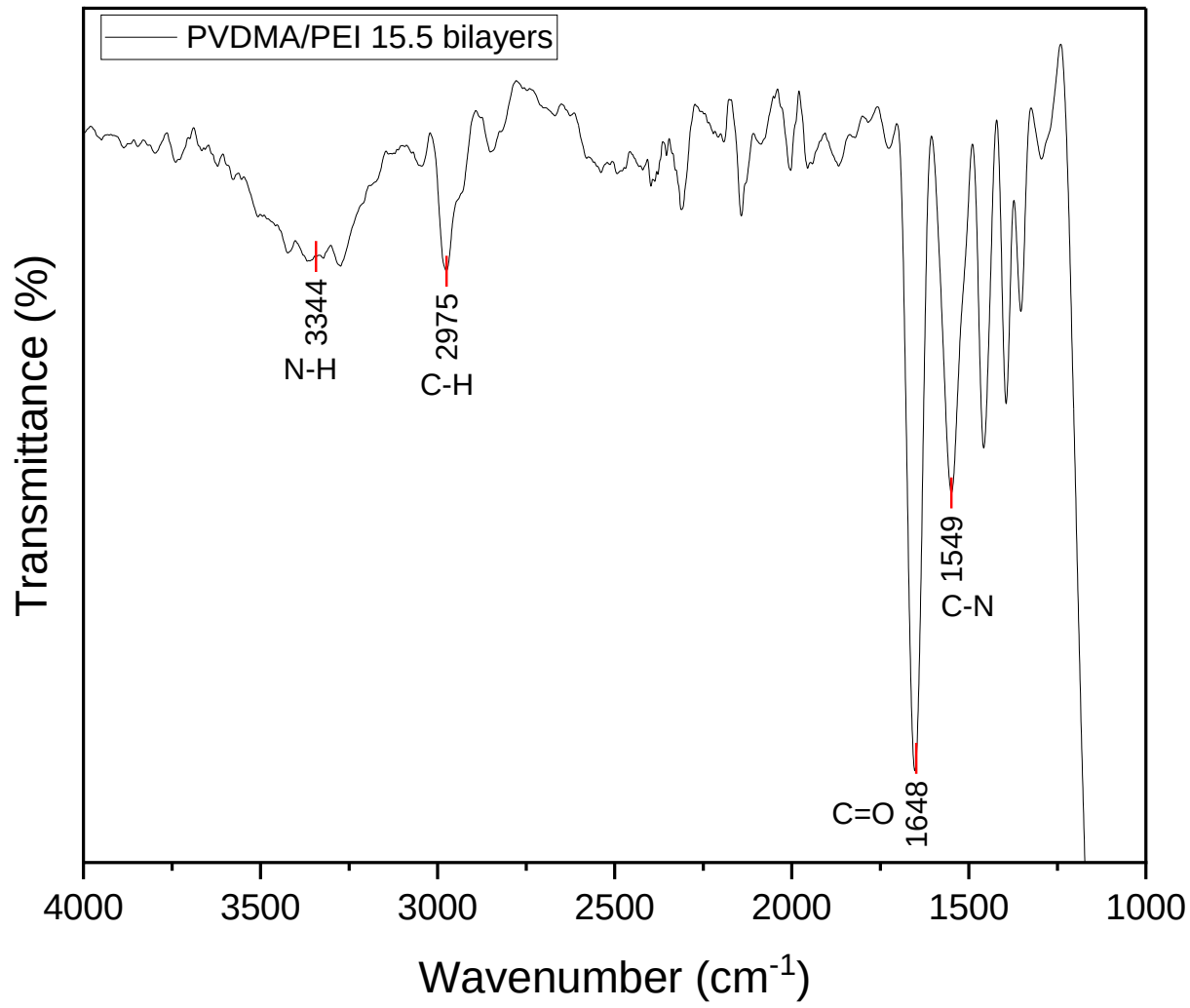

Figure S36. FTIR spectrum of 15.5 bilayer PVDMA/PEI.

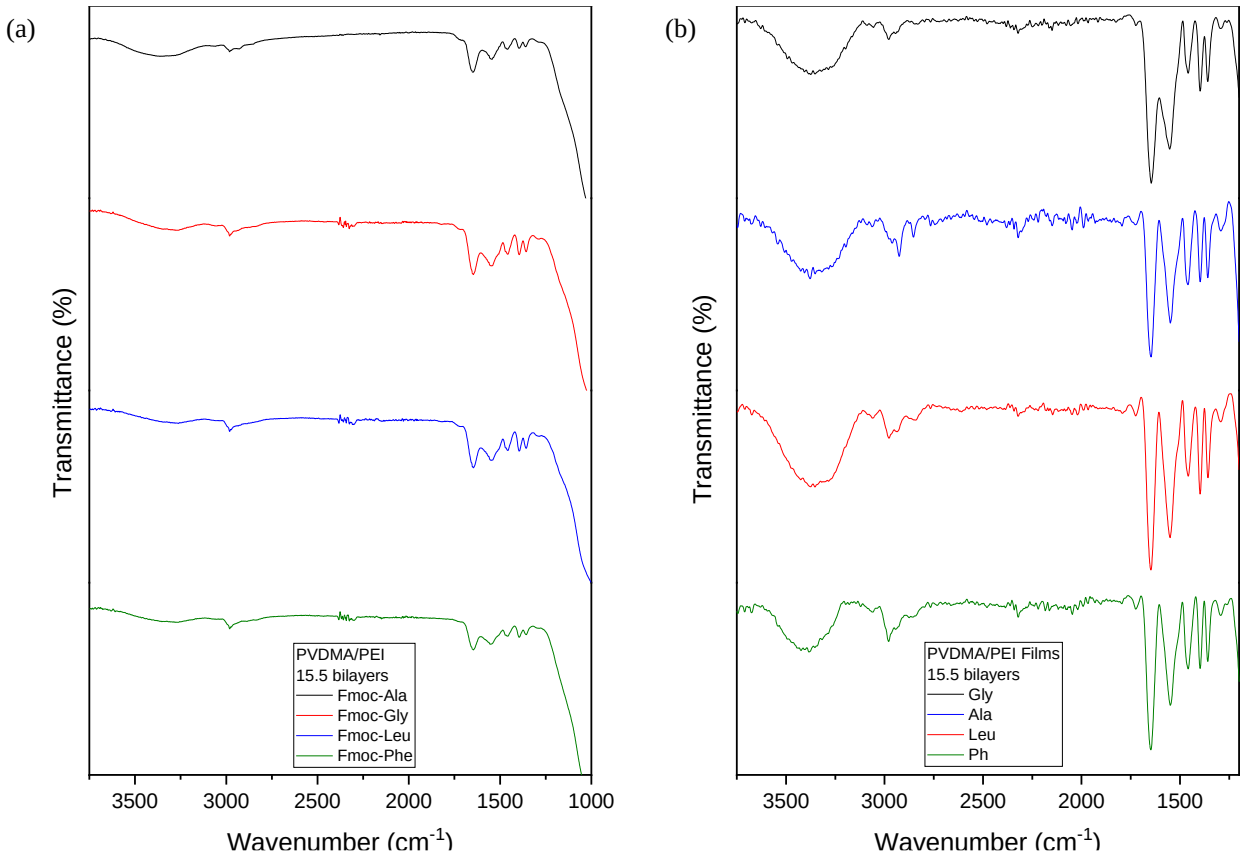

Figure S37. FTIR spectrum of PVDMA/PEI functionalized with (a) Fmoc-protected and (b) unprotected amino acids.

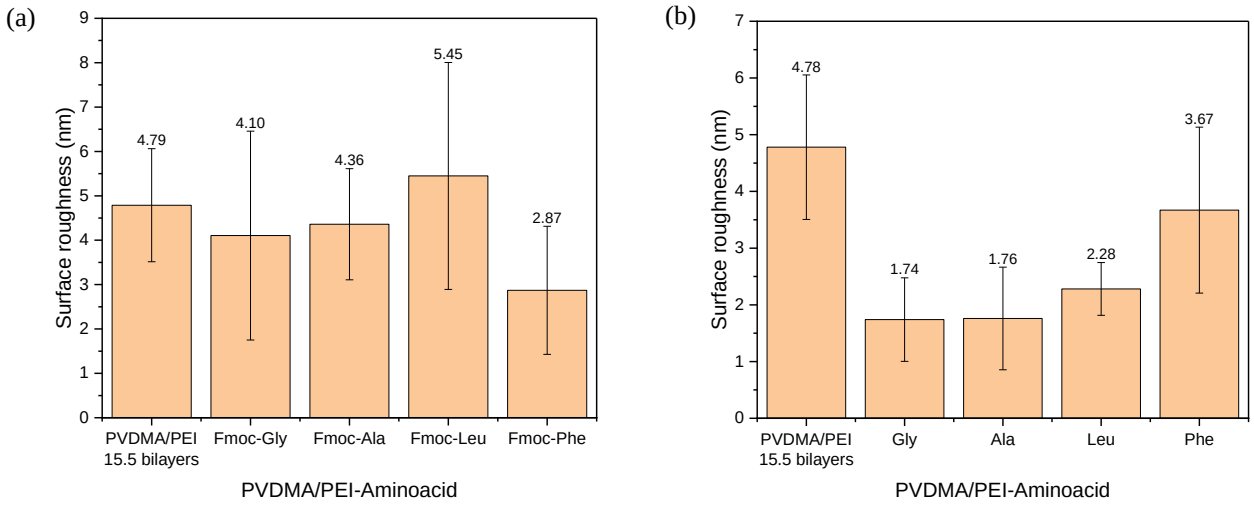

Figure S38. Arithmetic mean surface roughness (Sa measured by AFM microscopy of PVDMA/PEI films functionalized with (a) Fmoc-protected amino acids and (b) unprotected amino acids

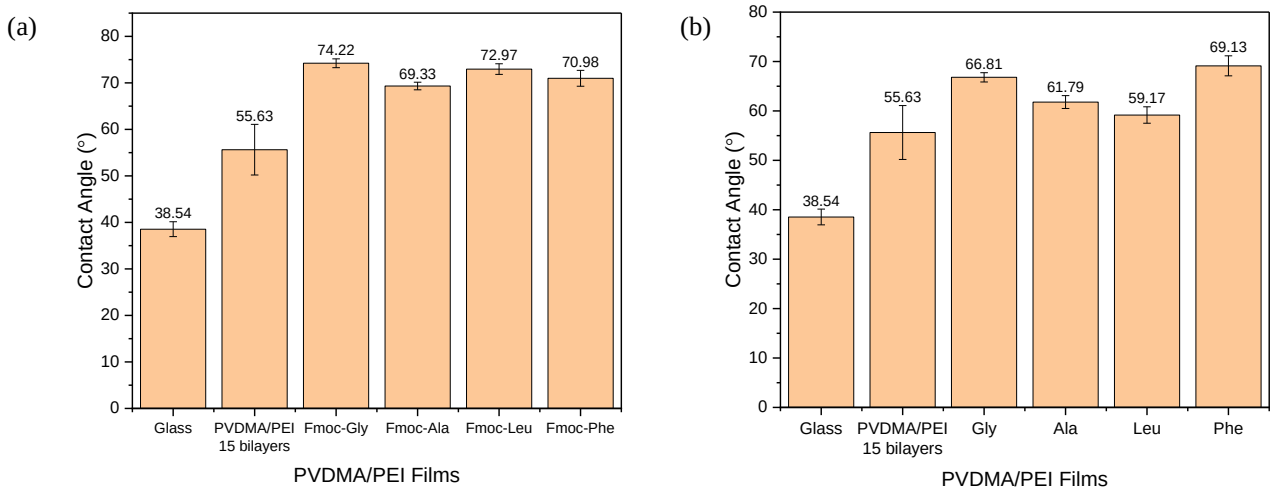

Figure S39. Contact angle values of PVDMA/PEI films functionalized with (a) Fmoc-protected amino acids and (b) unprotected amino acids.

Parameter	Energy (KJ/mol)	ΔE (KJ/mol)	Image
Phospholipid (PL)	-343.27	0.0	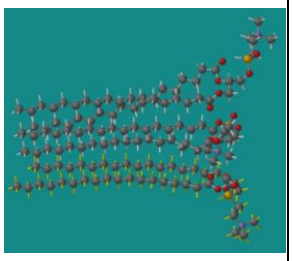
PL+F-Gly	-221.05	+122.22	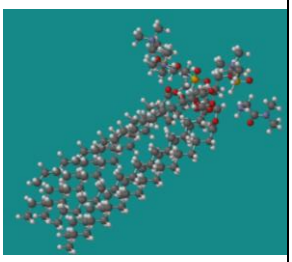
PL+F-Ala	-249.95	+93.32	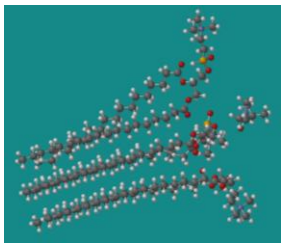
PL+F-Leu	-77.87	+265.40	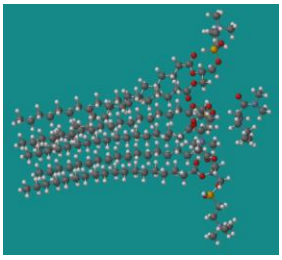
PL+F-Phe	-143.02	+200.07	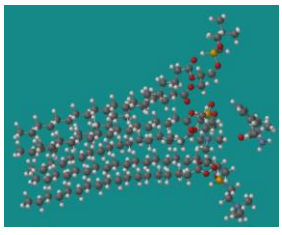

Figure S40. Optimization by molecular dynamics between the phospholipid and the interaction with the amino acids that is on the surface of the film.[1]

Reference

1. *Spartan*'14; Wavefunction Inc: Irvine, CA, 2021. [Link] accessed in January 2026